Available online at www.sciencedirect.com
ScienceDirect
Journal of Molecular Catalysis A: Chemical 277 (2007) 233–251
JOURNAL OF MOLECULAR CATALYSIS A: CHEMICAL
www.elsevier.com/locate/molcata

Catalytic deoxygenation of terminal-diols under acidic aqueous conditions by the ruthenium complexes $[(\eta^6\text{-arene})Ru(X)(N \cap N)](OTf)_n$, X = H_2O, H, η^6-arene = *p*-Me-^{i}Pr-C_6H_4, C_6Me_6, N ∩ N = bipy, phen, 6,6′-diamino-bipy, 2,9-diamino-phen, *n* = 1, 2) Influence of the *ortho*-amine substituents on catalytic activity

Ryan R. Dykeman [a], Kylie L. Luska [a], Michelle E. Thibault [a], Matthew D. Jones [a], Marcel Schlaf [a,*], Monther Khanfar [b], Nicolas J. Taylor [c,✠], James F. Britten [d], Laura Harrington [d]

[a] *Department of Chemistry, University of Guelph, The Guelph-Waterloo Center for Graduate Studies in Chemistry (GWC)^2, Guelph, Ontario N1G 2W1, Canada*
[b] *The University of Jordan, Chemistry Department, Amman 11942, Jordan*
[c] *Department of Chemistry, The Guelph-Waterloo Center for Graduate Studies in Chemistry (GWC)^2, University of Waterloo, 200 University Avenue West, Waterloo, Ontario N2L 3G1, Canada*
[d] *Department of Chemistry, McMaster Analytical X-Ray Diffraction Facility (MAX), McMaster University, Hamilton, Ontario L8S 4M1, Canada*

Received 5 July 2007; received in revised form 7 August 2007; accepted 8 August 2007
Available online 12 August 2007

Abstract

A series of ruthenium complexes of the general composition $[(\eta^6\text{-arene})(N \cap N)Ru(X)](Y)_n$, (arene = *p*-Me-^{i}Pr-C_6H_4, C_6Me_6; N ∩ N = bipy, phen, 6,6′-diamino-2,2′-bipyridine, 2,9-diamino-1,10-phenanthroline; X = Cl, H, H_2O; Y = Cl, OTf) was synthesized and the new compounds exhaustively structurally characterized by standard techniques (NMR, IR, elemental analysis, single-crystal X-ray crystallography). The single-crystal X-ray structures of [(*p*-Me-^{i}Pr-C_6H_4)Ru(dabipy)Cl][Cl] (**3Cl[Cl]**), [(*p*-Me-^{i}Pr-C_6H_4)Ru(daphen)Cl][Cl] (**4Cl[Cl]**), [(C_6Me_6)Ru(dabipy)Cl][Cl] (**7Cl[Cl]**), [(C_6Me_6)Ru(daphen)Cl][Cl] (**8Cl[OTf]**), [(*p*-Me-^{i}Pr-C_6H_4)Ru(bipy)(H_2O)][OTf]$_2$ (**1O[OTf]$_2$**), [(*p*-Me-^{i}Pr-C_6H_4)Ru(dabipy)(H_2O)][OTf]$_2$ (**3O[OTf]$_2$**), [(*p*-Me-^{i}Pr-C_6H_4)Ru(dabipy)(H_2O)][SO_4] (**3O[SO_4]**), [(*p*-Me-^{i}Pr-C_6H_4)Ru(daphen)(H_2O)][OTf]$_2$ (**4O[OTf]$_2$**), [(C_6Me_6)Ru(daphen)(MeOH)][OTf]$_2$ (**8(MeOH)[OTf]$_2$**), [(*p*-Me-^{i}Pr-C_6H_4)Ru(dabipy)(H)][OTf] (**3H[OTf]**), [(*p*-Me-^{i}Pr-C_6H_4)Ru(daphen)(H)][OTf] (**4H[OTf]**), [(C_6Me_6)Ru(dabipy-BH_2-OTf)(H)] (**7H[-NH_2-BH_2-OTf]**) have been determined. Under 750–1100 psi (5–7.5 MPa) of hydrogen pressure at 110 °C in the presence of acid and water in sulfolane solvent the aquo complexes form active catalysts for the selective deoxygenation of terminal diols, notably 1,2-hexanediol, to the corresponding primary alcohol, i.e., 1-hexanol in up to 60% yield. The presence of amino functions on the *ortho*-positions of the chelating ligands results in lower catalyst activity. Under the same reaction conditions the catalysts fail to convert glycerol to GC-detectable products. At the higher temperatures (T > 150 °C) possibly required for glycerol activation the catalysts show increasing decomposition with increasing temperature.
© 2007 Elsevier B.V. All rights reserved.

Keywords: Hydrogenation; Ruthenium; Diol; Deoxygenation; Glycerol

1. Introduction

The selective deoxygenation of terminal diols to primary alcohols is one of the fundamental reactions required for the conversion of renewable sugar polyalcohols to the corre-

* Corresponding author. Tel.: +1 519 824 4120x53002; fax: +1 519 766 1499.
E-mail address: mschlaf@uoguelph.ca (M. Schlaf).
✠ Deceased.

1381-1169/$ – see front matter © 2007 Elsevier B.V. All rights reserved.
doi:10.1016/j.molcata.2007.08.008

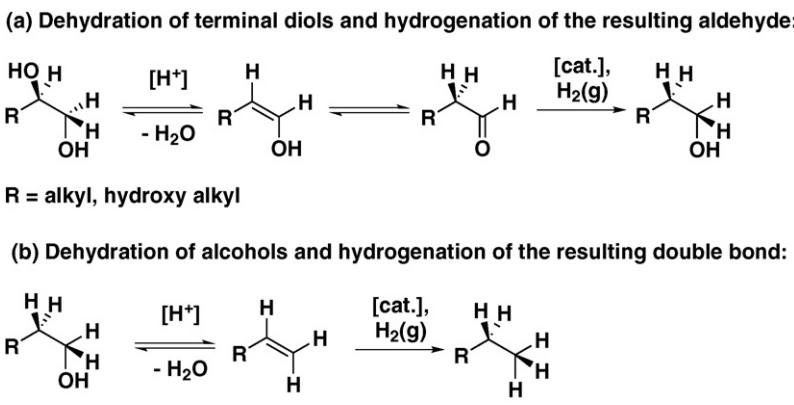

Scheme 1. Reaction pathways for the deoxygenation of terminal diols to primary alcohols (a) and subsequent possible total hydrogenation to alkanes (b).

sponding α,ω-diols, which could directly serve as polyester and polyurethane components. An economically very attractive example of such a transformation would be the selective deoxygenation of the bio-Diesel by-product glycerol [1] to 1,3-propanediol. One principle strategy to achieve this goal is an acid-catalyzed dehydration of a terminal diol function to an aldehyde, followed by a homogeneously metal-catalyzed hydrogenation in the same reactor vessel. Scheme 1 illustrates this reaction pattern (a) along with the less desirable potential follow-up reaction (b) leading to a total deoxygenation of the diol to the corresponding alkane. Reaction (a) constitutes a necessary – albeit not sufficient – criterion for catalyst activity in the desired glycerol deoxygenation. We recently discussed the challenges and opportunities of this strategy in detail [2].

To date only two homogeneous catalyst systems employing this strategy and capable of catalyzing the deoxygenation of glycerol have been described: in NMP solvent the system HWO_4/(acac)$Rh(CO)_2$ yields up to ∼20% 1,3-propanediol along with about the same amount of 1,2-propanediol and traces of *n*-propanol after 24 h at 200 °C and 4600 psi (31.7 MPa) pressure of a 1:2 mixture of CO(g) and H_2(g) [3]. The combination of HCl, methyl sulfonic acid and $(R_2PCH_2CH_2PR_2)Pd(OAc)_2$ (R = 1-cyclooctenyl or *sec*-butyl) in sulfolane/water mixtures yields <5% 1,3-propanediol along with traces of 1,2-propanediol and substantial amounts of *n*-propanol and acrolein after 10 h at 175 °C and 900 psi (6.2 MPa) of a 1:2 mixture of CO(g) and H_2(g) [4]. Presumably the use of synthesis gas rather than pure hydrogen in both cases stabilizes the catalysts at the – for homogeneous systems – comparatively high reaction temperatures. Neither system has found practical applications. Heterogeneous catalysts that convert glycerol to 1,2-propanediol with high selectivity and in some case good yield exist [5–9] and are being commercialized [10], but to the best of our knowledge no heterogeneous system to date has been described that can generate the more valuable 1,3-propanediol in meaningful yields. The high selectivity of heterogeneous catalysts is likely caused by the preferential reaction of one of the sterically more accessible terminal hydroxyl groups with an acidic catalyst surface resulting in dehydration to acetol followed by hydrogenation to 1,2- rather than 1,3-propanediol [11]. Scheme 2 illustrates this concept.

We therefore postulate that any catalyst capable of deoxygenating glycerol to 1,3-propanediol will have to be homogeneous in nature, exploiting the relatively higher stability of a secondary carbo-cationic intermediate formed by loss of water from the secondary position of glycerol under acidic conditions in a polar reaction medium. This dehydration gives 3-hydroxypropionaldehyde as the key intermediate [12,13], which can in situ be hydrogenated to 1,3-propanediol. While no mechanistic data is available from the patents, the two homogeneous catalyst systems mentioned above very likely operate by this pathway. Following the same strategy, we previously evaluated two ruthenium based homogeneous catalyst systems for the selective deoxygenation of terminal diols to primary alcohols [2,14,15], leading us to formulate a set of rational catalyst design criteria that any catalyst system will have to fulfill in order to be potentially viable for the deoxygenation strategy summarized in Scheme 1. Most importantly, the criteria demand that the catalyst be capable of heterolytic activation of hydrogen gas, resulting in a ionic hydrogenation mechanism, and be tolerant of the acidic and by definition aqueous reaction conditions. Following these design criteria and inspired by the work of Ogo and Süss-Fink, we identified the complexes of the general composition $[(\eta^6\text{-arene})Ru(H_2O)(N \cap N)](OTf)_2$, ($\eta^6$-arene = *p*-cymene, C_6Me_6, N ∩ N = bipy, phen) as potentially viable catalyst precursors for the deoxygenation of terminal diols and ultimately glycerol under acidic aqueous conditions. Ogo and Süss-Fink had previously shown that these complexes are active for both the transfer hydrogenation of ketones by formate under aqueous acidic con-

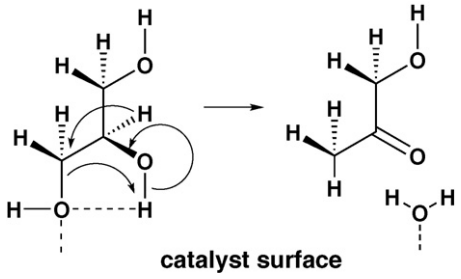

Scheme 2. Possible origin of the high selectivity of glycerol dehydration to acetol on a heterogeneous catalyst surface.

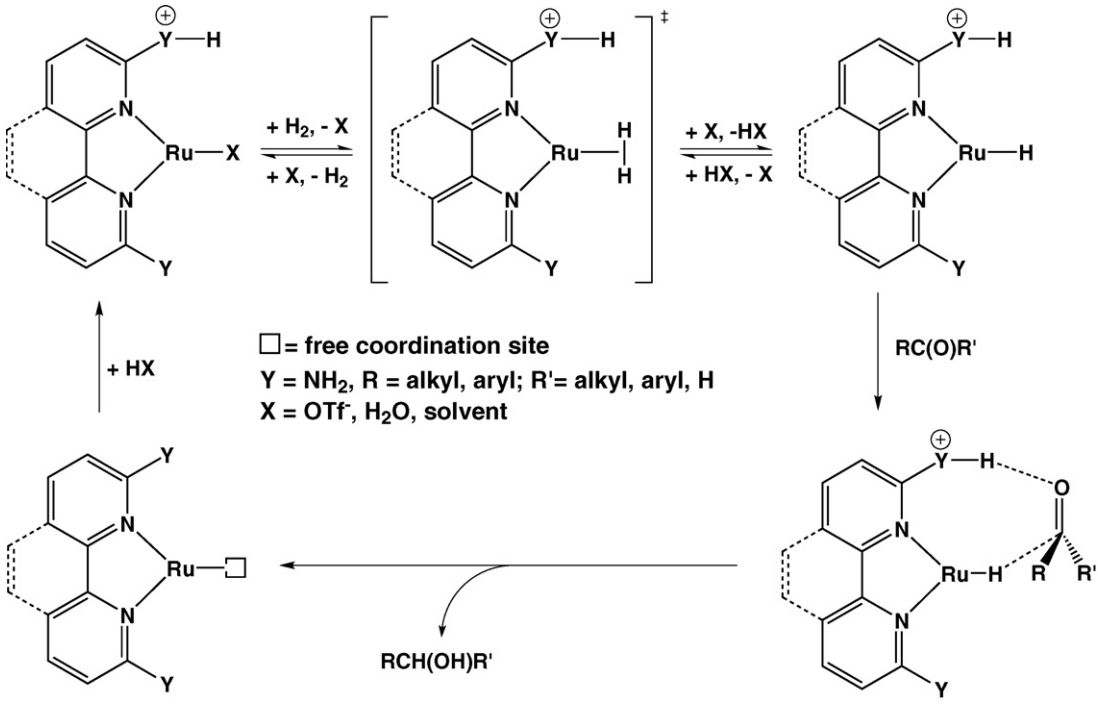

Scheme 3. Hypothetical catalytic cycle for a metal–ligand bifunctional ionic hydrogenation of carbonyl functions by (η^6-arene)Ru(H)(N∩N)(OTf), (η^6-arene = *p*-cymene, C_6Me_6, N∩N = 6,6′-diamino-2,2′-bipyridine or 2,9-diamino-1,10-phenanthroline). The η^6-arene ligand is omitted for clarity.

ditions [16–18] and the hydrogenation of CO_2 to formate using H_2(g) [19–21].

In an attempt to rationally design a more active catalyst system, we also hypothesized that the introduction of amino functions in the *ortho*-positions of the chelating ligands, i.e., the use of 6,6′-diamino-2,2′-bipyridine instead of 2,2′-bipyridine or 2,9-diamino-1,10-phenanthroline instead of 1,10-phenanthroline would result in more active catalysts by opening a pathway to a metal–ligand bifunctional concerted hydrogenation as pioneered by Shvo and co-workers [22–24] and Morris and co-workers [25–28] for hydrogenation and Noyori for transfer hydrogenation catalysts [29,30]. Scheme 3 illustrates the concept for the complexes studied here. The mechanism postulates a heterolytic activation of hydrogen gas by a non-classical dihydrogen complex and a proton shuttle role for the *ortho*-amino substituents resulting in the close spatial positioning of a hydride (Ru–H) and a proton source ($-NH_3^+$) in the coordination sphere of the catalytic centre.

Here we describe the synthesis of both the parent and aminated bipy and phen supported catalysts and their evaluation in the catalytic hydrogenation of acetophenone and benzophenone and the deoxygenation of 1,2-hexanediol and glycerol.

2. Results

2.1. Synthesis and structures of the catalysts

The structures of the complexes synthesized and evaluated as catalysts are shown in Chart 1 with their numbering scheme **#O** denoting the aquo, **#Cl** chloro and **#H** the hydride complexes, respectively. Complexes **1O** and **5O** have previously been described as the PF_6^- salts [31] and **2O** and **6O** as the BF_4^- salts [16,17]. The synthesis of all triflate counter ion complexes described here was carried out by reacting either [$RuCl_2(\eta^6$-*p*-Me-^{i}Pr-$C_6H_4)]_2$ [32] or [$RuCl_2(\eta^6$-$C_6Me_6)]_2$ [33], with the chelating ligand and a slight excess of AgOTf.

Depending on the order of addition either the corresponding chloro complexes [(η^6-arene)Ru(Cl)(N∩N)]Cl (ligand

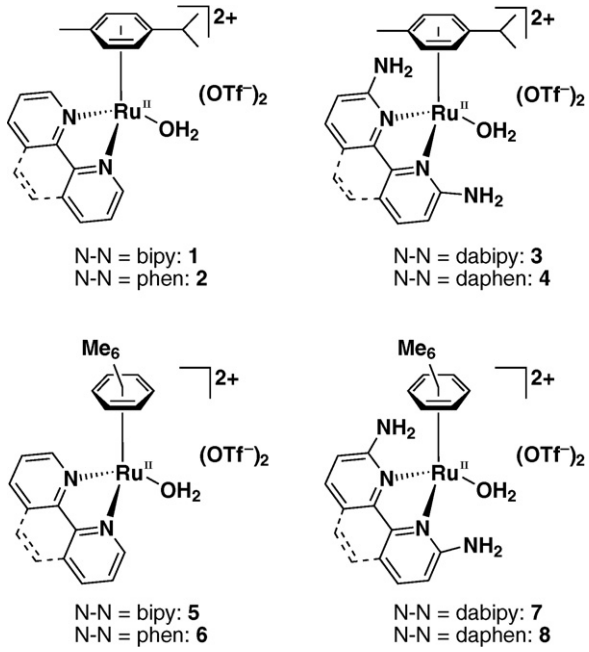

Chart 1. Structures of the eight aquo complexes of the type [(η^6-arene)Ru(N∩N)(H_2O)](OTf)$_2$ (**1O[OTf]$_2$–8O[OTf]$_2$**) synthesized and tested as catalysts.

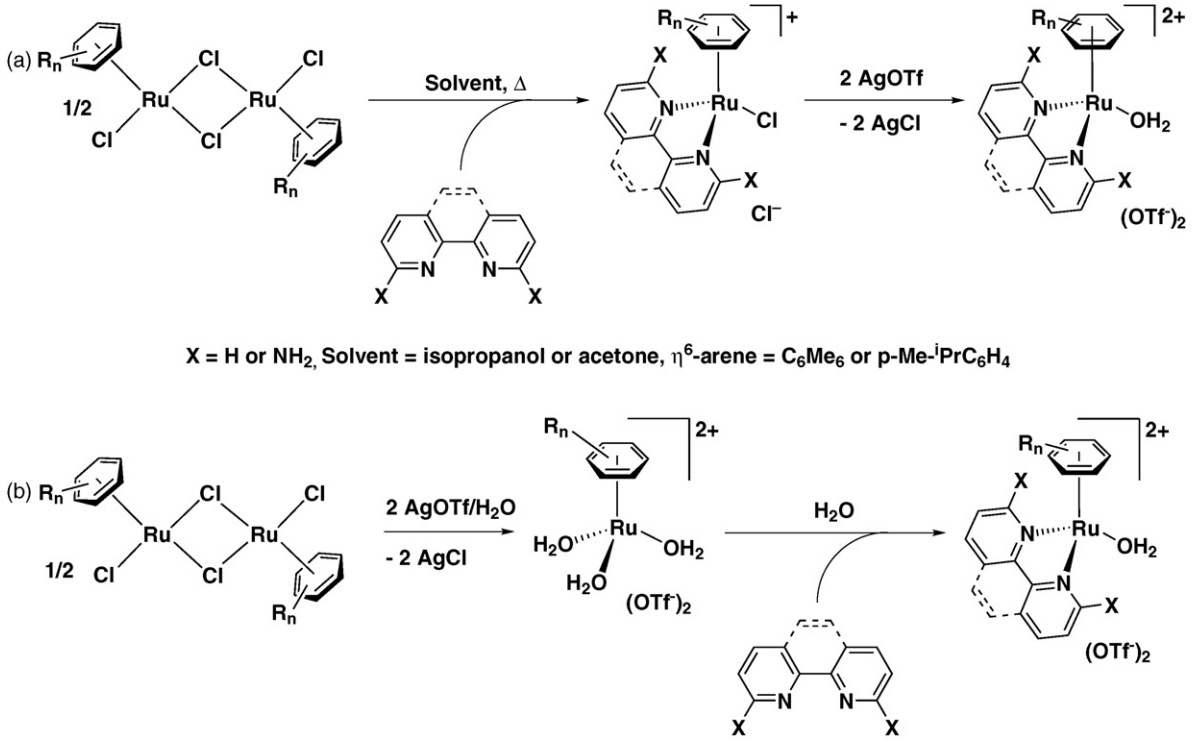

Scheme 4. Synthetic routes to the aquo complexes $[(\eta^6\text{-arene})Ru(N\cap N)(H_2O)](OTf)_2$. (a) Chloro route and (b) aquo route.

addition first → *chloro route*) or the triaquo complexes $[(\eta^6\text{-arene})Ru(H_2O)_3](OTf)_2$ [34] (AgOTf addition first → *aquo route*) are formed as intermediates. The two synthetic routes are shown in Scheme 4. Typically the chloro complexes are isolated, while the triaquo complex is reacted with the ligand in situ after removal of the AgCl formed in the first step by filtration and exchange of the aqueous solvent for methanol. After empirical optimization the complexes **1O[OTf]$_2$**, **1O[SO$_4$]**, **3O[OTf]$_2$**, **4O[OTf]$_2$**, and **7O[OTf]$_2$** were prepared via the *chloro route* with isolation (and for new complexes full characterization) of the intermediate chloro complexes. **5O[OTf]$_2$** [16] was prepared by both routes. The remaining complexes **2[OTf]$_2$** [17], **3O[SO$_4$]**, **6O[OTf]$_2$** [17] and **8O[OTf]$_2$** were prepared by the aquo route following literature procedures for the known complexes, but exchanging the silver salts used for AgOTf where applicable. The triflate complexes gave NMR spectra identical to those reported for the corresponding PF_6^- or BF_4^- complexes previously reported. For the purpose of catalytic reactions we selected the triflate anion as it has higher resistance to thermal and hydrolytic degradation in the aqueous acidic reaction conditions used (vide infra).

The corresponding hydride complexes **1H[OTf]**–**8H[OTf]** were prepared through reaction of the aquo complexes with $NaBH_4$ in methanol. Complex **5H[OTf]** has been structurally characterized [20] while complex **6H[OTf]** could only be prepared in situ by Süss-Fink and co-workers, but not isolated in pure form [17]. We experienced the same for **1H[OTf]** and **2H[OTf]**, both of which could only be prepared in situ in a mixture with the corresponding hydroxy complexes $[(p\text{-Me-}^i\text{Pr-}C_6H_4)Ru(N\cap N)(OH)](OTf)$ and other unidentified products. In contrast, all amino-substituted hydride complexes **3H[OTf]**, **4H[OTf]**, **7H[OTf]** and **8H[OTf]** precipitated from the reaction solution giving satisfactory elemental analysis and in some cases single crystals suitable for X-ray analysis. The characteristic spectroscopic data of the hydride ligand in complexes **1H[OTf]**–**8H[OTf]** as recorded in methanol solvent are summarized in Table 1.

For the complexes **1O[OTf]$_2$**, **3O[OTf]$_2$**, **3H[OTf]**, **3Cl[OTf]** (obtained adventitiously during an initial attempt to prepare **3O[OTf]$_2$** via the *chloro route*), **4O[OTf]$_2$**, **4H[OTf]**, **4Cl[Cl]** and **8Cl[Cl]** single-crystal X-ray analysis was performed. Instead of the aquo complex **8O[OTf]$_2$** the methanol complex $[(C_6Me_6)Ru(daphen)(MeOH)][OTf]_2$ **8(MeOH)[OTf]$_2$** was obtained. Fig. 1(a) shows the cation struc-

Table 1
Characteristic spectroscopic data for the hydride ligand in complexes of the type $[(\eta^6\text{-arene})(N\cap N)Ru(H)][OTf]$ (**1H[OTf]–8H[OTf]**)

Complex	δ(Ru–H) [ppm], CD_3OD	ν(Ru–H) [cm^{-1}], CH_3OH
1H (bipy/*p*-Me-^{i}Pr-C_6H_4)[a]	−5.53[d]	1905[d]
2H (phen/*p*-Me-^{i}Pr-C_6H_4)[b]	−5.50[d]	1911[d]
3H (dabipy/*p*-Me-^{i}Pr-C_6H_4)[a]	−5.99	1884
4H (daphen/*p*-Me-^{i}Pr-C_6H_4)[a]	−5.61	1889
5H (C_6Me_6/bipy)[c]	−6.71[a,d]	1899[a,d]
6H (C_6Me_6/phen)[b]	−6.69[d]	1899[d]
7H (C_6Me_6/dabipy)[a]	−6.34	1849
8H (C_6Me_6/daphen)[a]	−6.02	1856

[a] This work.
[b] Ref. [17].
[c] Ref. [20].
[d] Complex not isolated—values determined in solution in presence of other species.

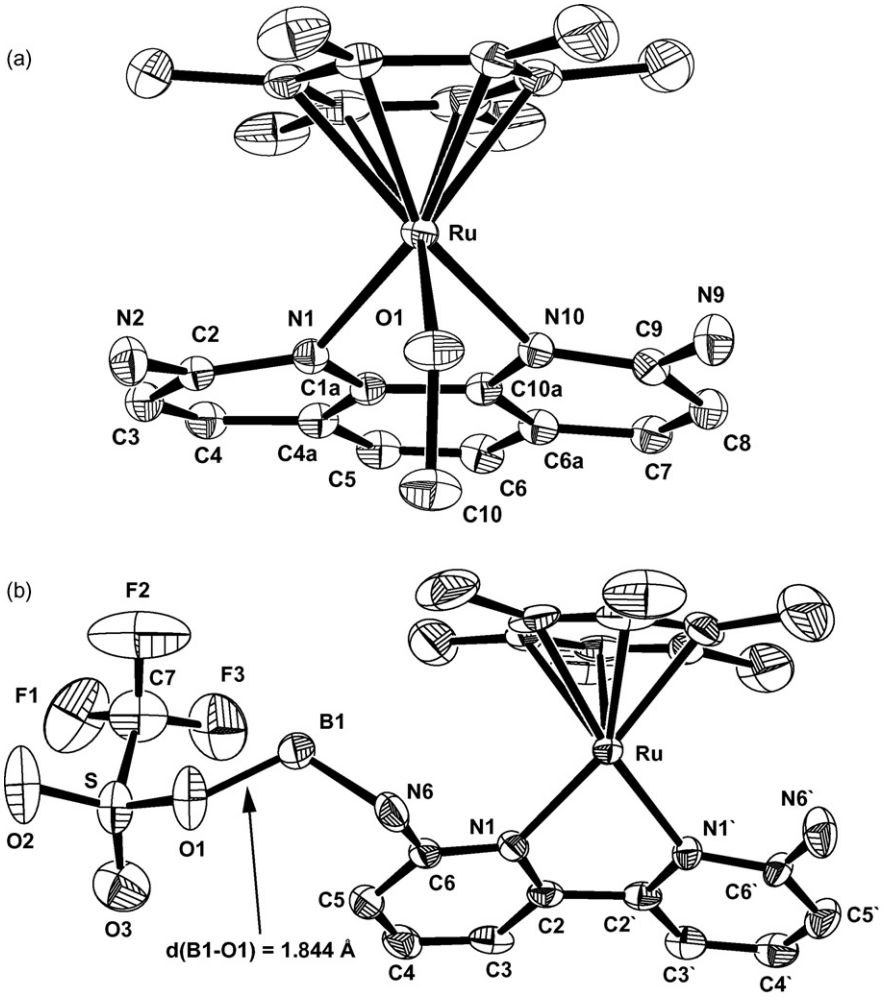

Fig. 1. ORTEP plots of (a) $[(C_6Me_6)Ru(daphen)(MeOH][OTf]_2$ **(8MeOH)[OTf]$_2$** and (b) $[(C_6Me_6)Ru(dabipy\text{-}BH_2\text{-}OTf)(H)]$ (**7H[-NH$_2$-BH$_2$-OTf]**) and drawn at 50% probability. Hydrogens and counter ions and solvent MeOH present in the structure of **(8MeOH)[OTf]$_2$** omitted for clarity.

ture of the methanol complex, in which the methyl group of the alcohol ligand is pointing down and away from the ruthenium centre, suggesting a minimal impact on the overall structure of the complex when compared to the corresponding aquo complex. A single crystal isolated from a reaction mixture of the preparation of the hydride complex **7H[OTf]** was determined to be an adduct of one of the amino functions of dabipy with -BH_2-OTf, representing an interesting artifact of the reduction of the aquo complex by $NaBH_4$. The structure is shown in Fig. 1(b). The boron–oxygen distance is 1.844 Å, i.e., substantially shorter than the sum of the van der Waals radii, suggesting a strong Lewis acid/base interaction. The hydride ligand could not be located in this structure.

Table 2 summarizes some characteristic bond length and angles of all these complexes as well as those of the earlier described complexes **5O[PF$_6$]$_2$**, **5H[OTf]**, and the η^6-benzene complex $[(C_6H_6)Ru(phen)Cl][Cl]$ (**9Cl**). Listed are the distances between the ruthenium centre and the nitrogen donor atoms in the bipy or phen chelate *d*(Ru–N), the distance between the ruthenium centre and the ligand X (X = Cl, H, OH_2) occupying the active site *d*(Ru–X), the distance between the ruthenium centre and the centroid of the η^6-arene ring *d*(Ru–C_6-centroid) and the angle α between the two planes defined the atoms N–C2–C2′–N′ of the bipy or N1–C1a–C10a–N10 for the phen chelate (cf. Fig. 1 for the numbering scheme) and the ruthenium centre (plane 1) and the six carbon atoms of the η^6-arene ring (plane 2). Reasonably assuming that the influence of the non-coordinating counter ions (OTf^-, BF_4^- or PF_6^-) on the structure of the ruthenium centred cations is negligible, a set of pairs of complexes emerge from the data in Table 2 that allow direct comparisons of the influence of the ligands *p*-Me-^{i}Pr-C_6H_4 vs. C_6Me_6, bipy vs. phen, bipy vs. dabipy and dabipy vs. daphen on the characteristic structural parameters while holding all other factors constant. The comparison of **1O** vs. **5O** reveals the influence of the nature of the arene ligand on the structure of the aquo complex procatalyst structure. With the sterically more demanding C_6Me_6 ligand all characteristic distances are longer by about ∼0.025 Å while the plane angle α is slightly smaller by about ∼4°, i.e., α is more acute. Both these observations can be rationalized on the basis of the higher steric demand of the C_6Me_6 ligand. The comparison between **5O** and **6O** (bipy vs. phen) gives a small effect on the characteristic bond distances and a slightly larger plane angle α (by ∼3.5°) for the phenanthroline ligand. The origin of this structural dif-

Table 2
Key structural data for complexes of the type [(η^6-arene)(N ∩ N)Ru(X)]Y_n, X = OH_2, H or Cl

Complex	N ∩ N	Y	*n*	*d*(Ru–N)[a]	*d*(Ru–X)[a]	*d*(Ru–C_6-centroid)[a]	α[a]
p-Me-^{i}Pr-C_6H_4							
1O[b]	Bipy	OTf	2	2.074	2.128	1.678	55.13
3O[b]	Dabipy	OTf	2	2.096	2.139	1.678	31.99
3SO$_4$[b]	Dabipy	SO_4	1	2.105	2.083	1.686	42.99
3H[b]	Dabipy	OTf	1	2.102	1.615	1.732	44.58
3Cl[b]	Dabipy	BF_4	1	2.096	2.401	1.682	33.72
4O[b]	Daphen	OTf	2	2.115	2.124	1.682	34.90
4H[b]	Daphen	OTf	1	2.102	1.610	1.718	46.55
4Cl[b]	Daphen	Cl	1	2.106	2.396	1.685	34.62
C_6Me_6							
5O[c]	Bipy	PF_6	2	2.098	2.153	1.695	51.73
5H[d]	Bipy	OTf	1	2.074	1.502	1.732	52.49
6O[e]	Phen	BF_4	2	2.110	2.166	1.697	55.20
7H[b,f]	Dabipy			2.096	–[f]	1.732	27.91
7Cl[b]	Dabipy	Cl	1	2.097	2.425	1.706	36.41
8O (MeOH)[b,g]	Daphen	OTf	2	2.138	2.142	1.697	34.21
8Cl[b]	Daphen	OTf	1	2.127	2.398	1.695	23.65
C_6H_6							
9Cl[e]	Phen	Cl	1	2.097	2.413	1.678	62.98

[a] Average over all equivalent bond distances/angles in the particular unit cell (either one or two symmetry equivalent complexes).
[b] This work.
[c] Ref. [16].
[d] Ref. [20].
[e] Ref. [17].
[f] Values from the F_3CSO_2O-BH_2-NH_2-bipy adduct. The hydride ligand could not be located in the structure.
[g] Values for the corresponding methanol complex **8(MeOH)[OTf]$_2$**.

ference is unclear. The most pronounced structural change is observed between the aminated and non-aminated complexes, e.g. **1O** vs. **3O** (non-aminated vs. aminated bipy ligand) that show a decrease of 23.14° in α induced by the steric repulsion between –NH_2 substituents in the *ortho* positions of the chelate and the η^6-arene ligand. This is illustrated in Fig. 2 that gives a "side-on" view of the two aquo complex procatalyst structures in both "stick" and space-filling representation. A further comparison emerging from the data in Table 2 is between **3H** and **4H** showing only minimal differences between the dabipy and daphen complexes with essentially no change in *d*(Ru–N), a 0.14 Å longer *d*(Ru–C_6-centroid) for dabipy matching the slightly smaller angle α (∼2°).

Fig. 3 shows the structure of the also prepared sulfate complex **3[SO$_4$]**, in which the sulfate dianion is coordinated to the ruthenium centre displacing the weakly coordinated water ligand observed with the triflate counter ions in **3O[OTf]$_2$**. The sulfate coordination in **3[SO$_4$]** is asymmetric with a close contact of 2.959 Å between N6 and O2 representing a hydrogen bond interaction between *o*-NH_2 and the sulfate anion. Further hydrogen bonds exist between O2 and a water molecule O5 at *d*(O2–O5) = 2.888 Å present in the second coordination sphere and between N6′ and O3 in adjacent complex in the lattice at *d*(N6′-O3) = 2.939 Å. The fact that no sulfate coordination is observed for the triaquo complex [(η^6-arene)Ru(H_2O)$_3$][SO_4] [16] suggests that such a stabilization through hydrogen-bond interaction between the *ortho*-amine functionality and an oxygen on the sulfate anion has to be present for coordination to occur.

2.2. Reactivity studies

As Scheme 3 shows, we postulated a non-classical η^2-H_2 complex generated by displacement of water as a reactive intermediate (or possibly transition state) in the heterolytic activation of hydrogen gas by the η^6-arene ruthenium complexes investigated here. This hypothesis was also formulated by Dyson et al. for the corresponding chelating phosphine complexes [(η^6-arene)(P ∩ P)Ru(Cl)]Cl (P ∩ P = dppe or similar) [35], which by necessity undergo loss of the chloride ligand under the reaction conditions. An alternative hydrogen activation model was given by Ogo and co-workers, who proposed a heterolytic activation of hydrogen through a concerted mechanism involving the coordinated water ligand and possibly ring-slippage to an η^4-coordinated arene ligand by generating a transient additional free coordination site on the ruthenium center [19]. These alternative mechanisms of hydrogen activation in aqueous media including a possible variant with metal–ligand bifunctional activation by an *ortho*-aminated chelate are shown in Scheme 5.

In an attempt to generate the η^2-H_2 complexes postulated in the catalytic cycle (Schemes 3 and 5) the two independently synthesized hydride complexes [(*p*-Me-^{i}Pr-C_6H_4)Ru(bipy)H]OTf (**1H[OTf]**) and [(*p*-Me-^{i}Pr-C_6H_4)RuH(dabipy)H]OTf (**3H[OTf]**) were reacted with HOTf in methanol-d_4 at room-temperature. In either case instantaneous formation of the aquo complexes and evolution of H_2 and HD gas was observed as indicated by their resonances in the ^{1}H NMR spectrum with their characteristic shifts and coupling constants (a singlet at 4.55 ppm and a 1:1:1 triplet at 4.51 with J_{HD} = 43 Hz, respec-

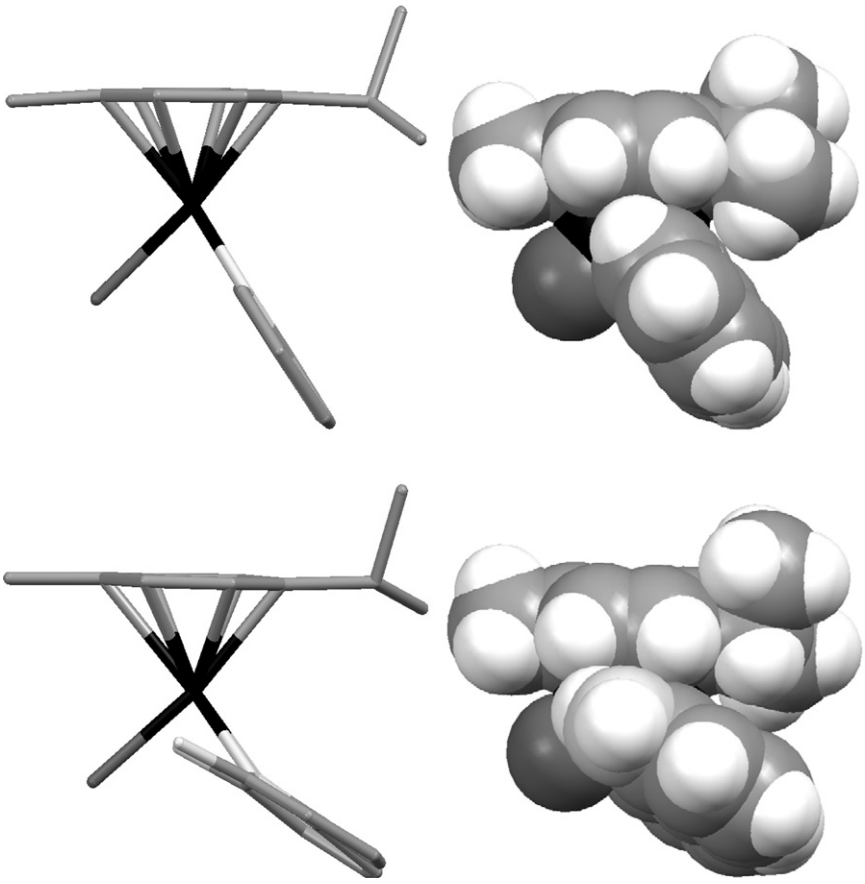

Fig. 2. Influence of the presence of the amino substituents on the angle α of the two rings in the cations **1O** vs. **3O** (non-aminated vs. aminated bipy ligand).

tively). Invoking the *Principle of Microscopic Reversibility*, the evolution of H_2(g) by protonation of the hydride complexes must be the reverse of the formation of the hydride complex from the aquo complex in the reaction mixture. This step is also directly mimicked by the generation of HD(g) by heating the procatalyst aquo species **1O[OTf]** or **3O[OTf]** under ∼3 atm of hydrogen gas atmosphere at ambient temperature, i.e., isotope exchange occurs between the gas phase and the perdeuterated solvent, which is only possible through either of the heterolytic H_2(g) activation pathways proposed in Scheme 5. If the sulfate complex **3[SO$_4$]** is employed in the same experiment heating to ∼70 °C is required to effect the generation of HD(g), suggesting that the hydrogen-bond supported sulfate coordination persists in solution at ambient temperature. Together these experiments provide evidence for a heterolytic activation of H_2(g), but do not allow a distinction between the two alternative pathways shown in Scheme 5. In a further attempt to directly observe an η^2-H_2 complex and possibly determine the characteristically short T_1 relaxation time of the typically broad resonance of an η^2-H_2 ligand [36] as well as the J_{HD} of its corresponding HD isotopomer [37], complexes **1H[OTf]** and **3H[OTf]** were reacted with excess HOTf in methanol-d_4 at −80 °C. However, even at this low temperature, no η^2-H_2 complex could be detected. Instead the resonance of the hydride ligand in either complex

Table 3
T_1 values obtained for [(*p*-Me-^{i}Pr-C$_6$H$_4$)Ru(bipy or dabipy)H]OTf

Compound	Temperature (°C)	Equivalents of HOTf[a]	T_1 measurement (s)
[(*p*-Me-^{i}PrC$_6$H$_4$)Ru(bipy)H]OTf	RT	0	2.20
	−80	0	1.52
	−80	1.5	1.48
	−80	15	1.65
	−60	15	1.17
	−60	15	0.82[b]
[(*p*-Me-^{i}PrC$_6$H$_4$)Ru(dabipy)H]OTf	RT	0	4.08
	−80	0	2.67
	−80	15	1.83

[a] With respect to ruthenium compound.
[b] T_1 value of the shoulder present on the upfield side of the hydride signal.

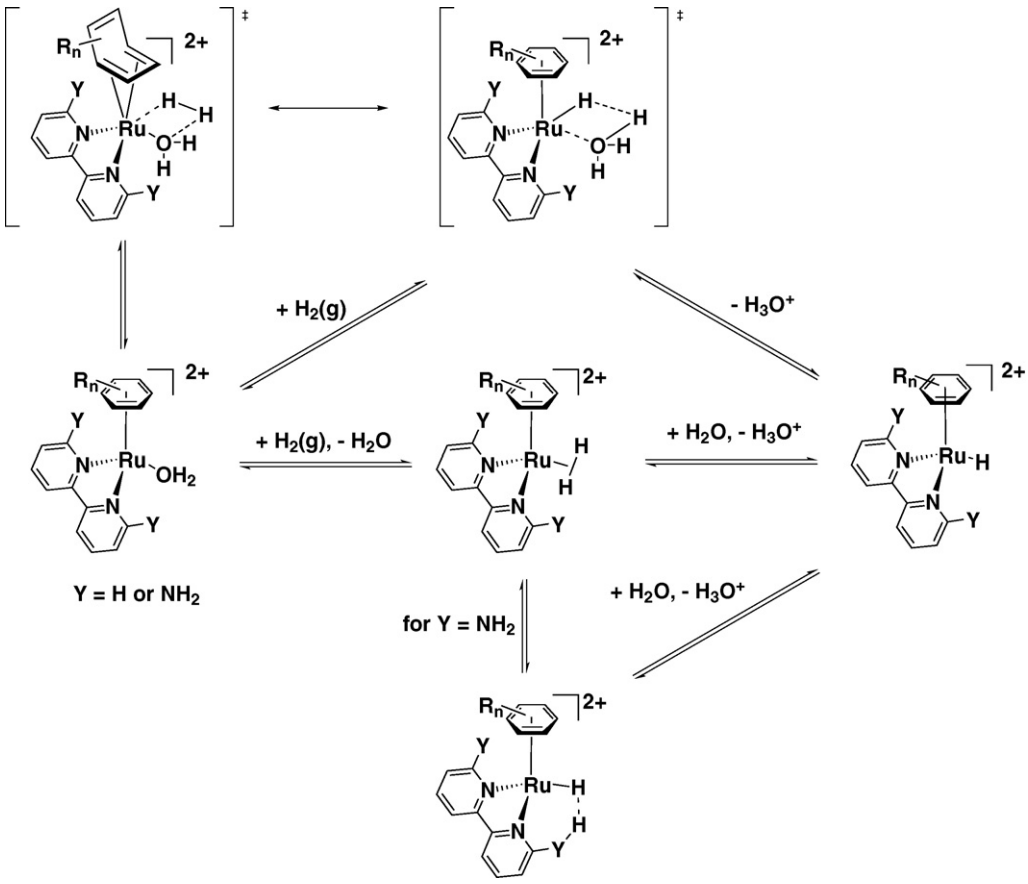

Scheme 5. Possible mechanisms of heterolytic hydrogen activation by the aquo procatalyst complexes.

remains sharp and its shift value almost unchanged up to −60 °C. The T_1 time of the hydride resonance is only marginally shorter than that of the hydride complex at ambient conditions, i.e., does not drop to the values of <100 ms expected for a non-classical dihydrogen complex. Table 3 lists the observed T_1 relaxation times as a function of temperature. Above −60 °C the hydride signal is lost and signals for free hydrogen and the aquo complexes **1O[OTf]$_2$** and **3O[OTf]$_2$** emerge. An interesting feature of the low-temperature spectrum of **1H[OTf]** is a shoulder peak appearing on the hydride signal in the presence of excess HOTf at −5.7 ppm at −80 °C. The T_1 time of this shoulder is slightly lower than that of the dominant hydride signal and shifted upfield, i.e., in the opposite direction expected for an η^2-H_2 ligand. We therefore propose that this shoulder peak originates form an interaction of the hydride ligand with an HOTf molecule in solution Ru–H···H–X$^{+/0}$ (X = H_2O, solvent or OTf^-) that on the reaction coordinate represents the first step to protonation and loss of H_2(g) observed upon warming. In contrast, a solution of the aminated ligand complex **3H[OTf]** under analogous conditions did not show a shoulder signal. Also its spectra gave no indication of a protonation of the amine substituents under these conditions.

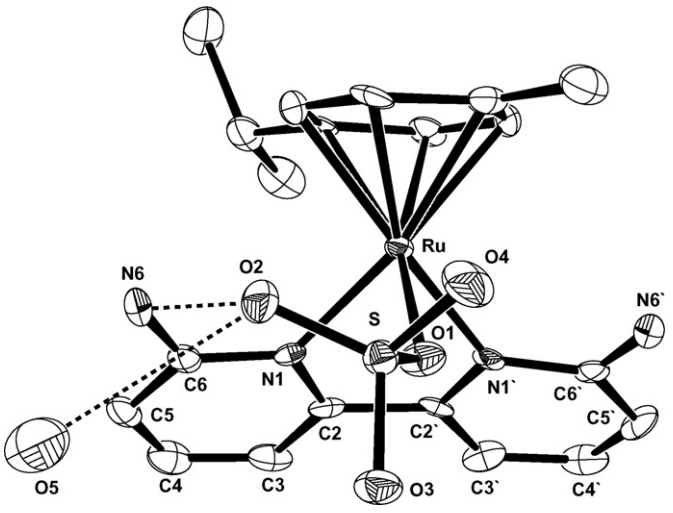

Fig. 3. Structure of the complex [(*p*-Me-^{i}Pr-C_6H_4)Ru(dabipy)(H_2O)][SO_4] (**3[SO$_4$]**).

The pK_a values of η^2-H_2 complexes are usually determined by establishing an equilibrium (Eq. (1)) between the corresponding hydride complex with an acid of known pK_a and measuring the relative concentration of the hydride and η^2-H_2 complex by integration of their NMR signals; this of course requires that the η^2-H_2 complex is stable and directly observable. With the pK_a of the external base known, the pK_a of the metal η^2-H_2 complex is easily calculated using Eq. (2) [37].

$$M(H_2) + B \leftrightarrow [M(H)L_x]^- + BH^+ \quad (1)$$

$$pK_a = pK_{eq} + pK_{BH^+} \quad (2)$$

Table 4
Effects of HOTf addition on the stability of [(*p*-Me-^{i}Pr-C_6H_4)Ru(bipy)H]OTf (**1H[OTf]**) in various deuterated solvents

Solvent	Observation	pK_a[a]
DMF-d_7	No protonation of hydride with ∼15 eq. HOTf	−0.5
CD_3OD	Shoulder peak with excess HOTf (T_1 ∼ 1 s/400 MHz)	−2
Acetone-d_6	Loss of hydride with ∼1.5 eq. HOTf	−7

[a] pK_a of the protonated NMR solvent on an aqueous scale.

Even without having established this equilibrium an approximate pK_a range for the postulated intermediate [(*p*-Me-^{i}Pr-C_6H_4)Ru(bipy)(η^2-H_2)]$^{2+}$ – or another protonated species of unknown structure derived from [(*p*-Me-^{i}Pr-C_6H_4)Ru(N∩N)H]OTf and HOTf – can be established by correlating the pK_a of the protonated NMR solvents used with the behaviour of the [(*p*-Me-^{i}Pr-C_6H_4)Ru(bipy)H]$^+$ cation under acidic conditions (Table 4). Upon the addition of HOTf to [(*p*-Me-^{i}Pr-C_6H_4)Ru(bipy)H]OTf (**1H[OTf]**) in acetone-d_6 at −80°, HD(g) is generated (Eqs. (3) and (4)). In contrast, when DMF-d_7 or methanol-d_4 were used as the solvent [RuH(bipy)(*p*-Me-^{i}Pr-C_6H_4)]OTf remained unprotonated (Eq. (5)).

$$RuH^+ \leftrightarrow Ru(H_2)^{2+} \quad (3)$$

$$Ru(H_2)^{2+} + X \rightarrow RuX^{+/2+}H_2(g) \quad (4)$$

$$RuH^+ + H^+ + Sol \leftrightarrow RuH^+ + SolH^+ \quad (5)$$

Extrapolating to the aqueous scale for which the pK_a values of the protonated solvents are known, the pK_a of the protonated species derived from [(*p*-Me-^{i}Pr-C_6H_4)Ru(bipy)H]OTf (**1H[OTf]**) must be between that of protonated acetone (pK_a = −7) and protonated methanol (pK_a = −2), though it can be speculated that it may be closer to that of methanol, assuming that it is an interaction of the hydride with the protonated solvent that leads to the shoulder peak on the hydride resonance observed in the NMR spectrum at low temperature. Ultimately, placing a numerical value on the pK_a of the protonated intermediate in this fashion is of course at best qualitative due to the use of only three solvents and the extrapolation to an aqueous pK_a scale. However, even a very approximate knowledge of the pK_a of the protonated species is valuable with respect to its catalytic activity under the aqueous reaction conditions that will level the overall acidity of the catalytic reaction mixtures to that of H_3O^+ (pK_a = −1.74 in aqueous media) [38] as the strongest acid present.

A result that logically emerges from the experiments described above (Table 4) is that the presence of the amine functions in [RuH(dabipy)(*p*-Me-^{i}PrC_6H_4)]OTf has no or little impact on the acid/base behaviour of the hydride complex, i.e., it appears that with 2 or more equivalents of HOTf either no protonation of the amines to [RuH(dabipyH)(*p*-Me-^{i}PrC_6H_4)](OTf)$_2$ occurs or if it does that the pK_a of such a species is low enough to protonate the hydride ligand leading to the immediate formation of a transient η^2-H_2 ligand and the subsequent observed irreversible loss of H_2(g) from the complex. This pegs the pK_a of a protonated *ortho*-amine bipyridine or phenanthroline ligand coordinated to ruthenium(II) at a remarkable −2 (aqueous scale) or possibly even lower. This low pK_a value may be the consequence of the already cationic hydride complex resisting the build-up further positive charge through protonation of the ligand. A direct titration of either the dicationic aquo complex [Ru(H_2O)(dabipy)(*p*-Me-^{i}PrC_6H_4)](OTf)$_2$ (**3O[OTf]$_2$**) or the monocationic [Ru(Cl)(dabipy)(*p*-Me-^{i}PrC_6H_4)]Cl (**3Cl**) with HOTf in aqueous medium while directly monitoring the pH of the solution with an electrode gives the same result, i.e., no protonation of the amine functions in the dabipy ligand is observable. Furthermore the titration curves of both **3O[OTf]$_2$** and **3Cl[OTf]$_2$** are identical to those obtained for the parent bipy complexes **1O[OTf]$_2$** and **1Cl[OTf]$_2$**, i.e., the presence of the amine substituent has no buffering effect on the pH of the solution as a function of acid added. Equivalent results are obtained when monitoring the UV/vis spectrum of the complexes as a function of added acid in aqueous solution, i.e., the spectra do not exhibit any distinct changes that could be associated with a protonation of the ligand. Since the strongest acid accessible in aqueous medium is H_3O^+ with a pK_a of −1.74, this confirms the estimate of −2 as the absolute upper limit for [(*p*-Me-^{i}PrC_6H_4)Ru(dabipyH)(H_2O)](OTf)$_3$ and [(*p*-Me-^{i}PrC_6H_4)(dabipyH)Ru(Cl)](OTf)$_2$ obtained from the NMR experiments discussed earlier. Some evidence that the amine functions can in fact serve as a proton shuttle as postulated in Scheme 3 comes from an NMR experiment, in which [(*p*-Me-^{i}PrC_6H_4)(dabipy)Ru(Cl)]Cl (**4Cl[Cl]**) was titrated with concentrated HCl in DMSO-d_6 solution, in which the chloro complex mimics the also monocationic hydride complex **4H**. DMSO-d_6 (ε = 48.9, μ = 3.9 D) was chosen as the NMR solvent as it most closely resembles the sulfolane medium (ε = 43.4, μ = 4.35 D) actually employed in catalytic reactions. Fig. 4 shows a series of ^{1}H NMR spectra of **4Cl[Cl]** illustrating the effect of the addition of ∼ 1 (5 μL), 2 (10 μL) and 4 (20 μL) equivalents (w.r.t. ruthenium) of concentrated HCl. Prior to the addition of acid both the amine substituents as well as water appear as well defined resonances at ∼7 and 3.3 ppm, respectively. As can be seen the resonance of the amine substituents at 7 ppm (overlapping with one of the ring protons of the ligand) broadens and shows increasing coalescence with the signal of $H_3O^+Cl^-$ that shifts from 4.8 to 5.3 ppm, indicating that in aqueous DMSO solution there is in fact rapid proton exchange taking place between these species.

2.3. Catalytic hydrogenation of ketones

Acetophenone and benzophenone were selected as the substrates for an initial evaluation of the relative activity and stability of **1O[OT]$_2$–4O[OTf]$_2$** as hydrogenation catalysts in sulfolane and to investigate the influence of the amine substituents on catalytic activity. The hydrogenation of acetophenone to 1-phenyl-ethanol is a standard reaction for the evaluation of homogeneous hydrogenation catalysts and was also employed by Süss-Fink and co-workers for the evaluation of the same or similar complexes as transfer hydrogenation catalysts in biphasic medium at pH 3.8 [17]. However, as Scheme 6 shows, a

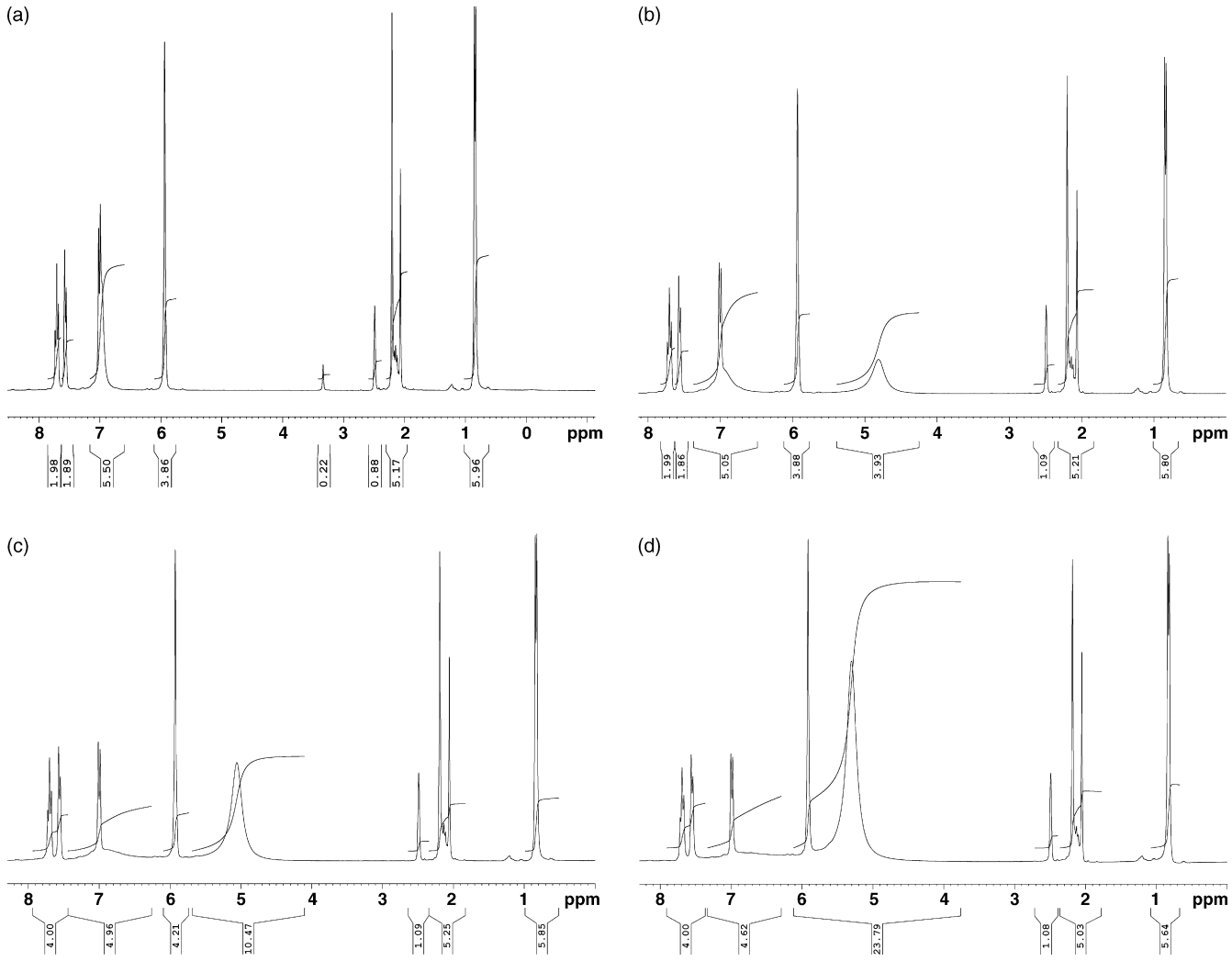

Fig. 4. NMR spectra showing rapid exchange of protons between $H_3O^+Cl^-$ and the amine functions in [Ru(Cl)(dabipy)(*p*-Me-^{i}PrC$_6$H$_4$)]Cl in DMSO-d_6 solvent. (a) No acid added; (b) 5 μL concentrated HCl added; (c) 10 μL concentrated HCl added; (d) 20 μL concentrated HCl added.

substantially more complex reaction cascade – triggered by a secondary water loss from the initial hydrogenation product 1-phenyl-ethanol to styrene followed by either total hydrogenation to ethyl benzene or styrene dimer- or oligomerization – evolves under the acidic conditions generated by the catalyst. The driving force for the secondary loss of water lies in the high solvation energy of water in the highly polar and hygroscopic sulfolane. The dehydration is catalyzed by HOTf – or more precisely under the reaction conditions $H_3O^+OTf^-$ – generated by the ruthenium catalyst through the heterolytic cleavage of hydrogen gas to the ruthenium hydride complex and free acid. Reaction conditions were 500 mmol/L of acetophenone with 0.5 mol% catalyst load for 24 h under 700 psi of H_2(g) at 50, 70 and 90 °C. The results of all catalytic runs carried out with this substrate at the 24 h time point are summarized in Table 5. Reaction mixtures were analyzed by quantitative GC against 100 mmol/L dimethyl sulfone added as an internal standard (ISTD) with multi-level calibrations against authentic standard solutions of acetophenone, 1-phenyl-ethanol, styrene and ethylbenzene. The identities of the other GC-detectable dimeric products bis(1-phenyl-ethyl)ether (BPE, diastereomeric mixture of *S*,*S*/*R*,*R* and *R*,*S*) and 1,3-diphenyl-1-butene (DPB) were determined by GC–MS and their amounts approximated using the same response factor as acetophenone. This introduces an error in the quantification that together with the formation of oligomers of styrene that cannot be analyzed by GC accounts for the incomplete/excess mass balance [MB] (in %) obtainable from the data in Table 5 as $[MB] = [AP] + [PE] + [ST] + [EB] + 2 \times [BPE] + 2 \times [DPB]$. For the higher temperatures an apparent loss of material of up to 45% of initial acetophenone occurs, which is attributed to the formation of involatile styrene oligomers. Ogo and co-workers had previously shown that the hydride complex [RuH(bipy)(η^6-C$_6$Me$_6$)](OTf) (**5O[OTf]**) is an effective styrene polymerization catalysts under aqueous acidic conditions [39]. Also conceivable is loss of the acetophenone substrate by dimerization through aldol condensation to 1,3-diphenyl-but-2-enone, which is however not observed in the GC traces. If it occurred it would upon iterative hydrogenation and loss of water also lead to DPB as the product, i.e., consume one hydrogenation equivalent per acetophenone lost. Due to the complexity of the overall reaction, the relative activity of the catalysts evaluated by the reactions listed in Table 5 is best compared by the total amount of hydrogen

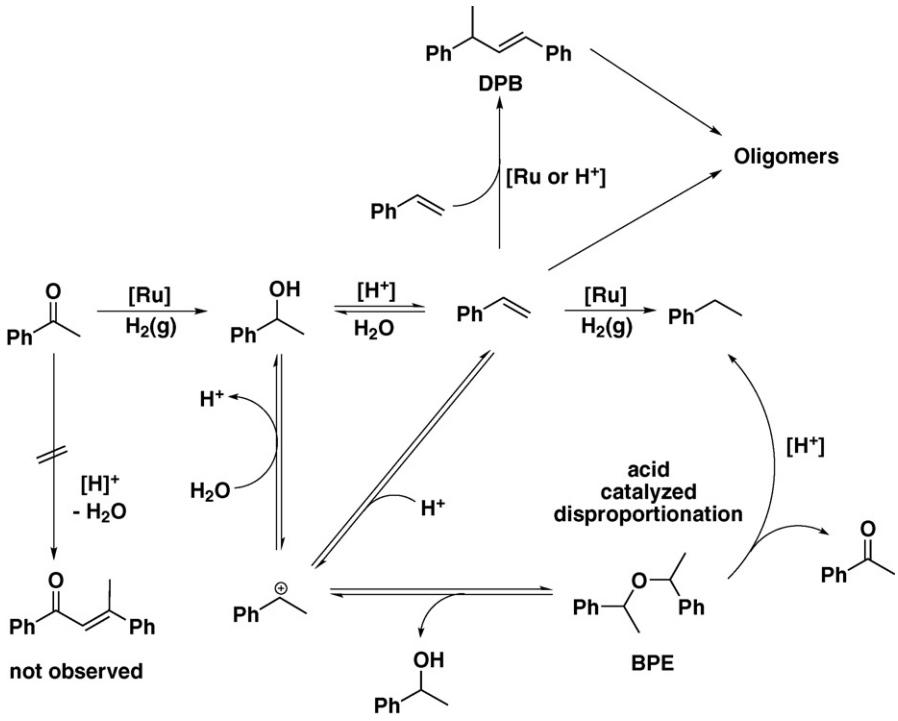

Scheme 6. Reaction cascade for the hydrogenation of acetophenone by in sulfolane medium.

consumed as defined by [100 − AP] + [EB] (in percent relative to the starting amount of acetophenone). This value includes the activity of the catalysts for the secondary hydrogenation of styrene to ethylbenzene and can therefore exceed 100%.

A much less complex reaction cascade is observed for benzophenone (Scheme 7). Table 6 summarizes the result of the catalytic runs for this substrate under the same reaction conditions. With the exception of bis(diphenylmethyl)ether, which cannot be analyzed by GC due to decomposition during injection causing the peak for the compound to recede into the baseline of the GC-trace, all the concentrations of all components of the reaction mixture, i.e., benzophenone (BP), diphenyl methanol (DOH) and diphenyl methane (DPM) were determined by quantitative GC with calibration against authentic solutions. The concentration of bis(diphenylmethyl)ether was inferred through the mass balance.

The appearance of diphenyl methane as the final product of the hydrogenation of benzophenone could in principle be interpreted as the result of a remarkable direct metal-catalyzed hydrogenolysis of either diphenyl methanol or bis(diphenyl)methyl ether. However, we exclude this possibility on the basis of the known high propensity of benzyl ethers to undergo acid-catalyzed disproportionation reactions [40] and the following observations: if diphenyl methanol is used as the substrate (entries 2 and 3, Table 6) benzophenone is detected in the reaction mixture. Under these conditions it can only originating from the disproportionation of the ether formed through condensation of two equivalents of diphenyl methanol. The analogous process occurs in the hydrogenation of acetophenone, where the GC-detectable bis(1-phenyl-ethyl)ether formed appears as a transient reaction mixture component in low concentration. Fig. 5 shows a typical 24 h reaction profile for the hydrogenation of acetophenone.

Examination of the hydrogenation data for acetophenone in Table 5 and benzophenone in Table 6 reveals that the percentage conversion to the total hydrogenation products ethylbenzene/DBP and DPM, respectively, scaled with the reaction temperature. They are therefore the thermodynamic products for this system. For the acetophenone hydrogenation (Table 5) a pair wise comparison of the total hydrogenation equivalents for *bipy* vs. *dabipy* and *phen* vs. *daphen* bearing metal centres reveals that the presence of the amine substituents has a detrimental rather than positive effect on catalyst activity for the bipy/dabipy pair and a marginally positive effect for the phen/daphen pair. In no case did the presence of the aminated ligand results in a substantial enhancement of catalyst activity postulated for an

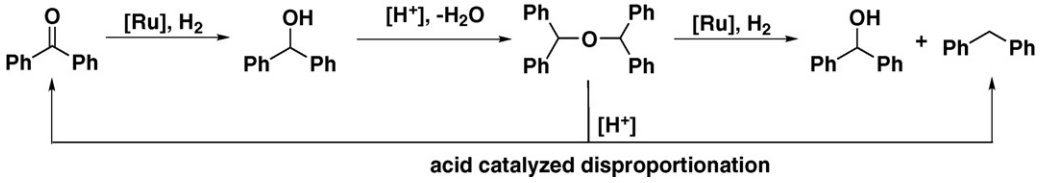

Scheme 7. Reaction cascade for the hydrogenation of benzophenone in sulfolane medium.

Table 5
Hydrogenation of acetophenone by $[Ru(H_2O)(N \cap N)(p\text{-Me-}^iPrC_6H_4)](OTf)_2$, N ∩ N = bipy, dabipy, phen or daphen

N ∩ N[a]	T [°C]																			
	50							70							90						
	AP[b] (%)	PE[b] (%)	ST[b] (%)	EB[b] (%)	BPE[c] (%)	DPB[c] (%)	H_2[d] (%)	AP[b] (%)	PE[b] (%)	ST[b] (%)	EB[b] (%)	BPE[c] (%)	DPB[c] (%)	H_2[d] (%)	AP[b] (%)	PE[b] (%)	ST[b] (%)	EB[b] (%)	BPE[c] (%)	DPB[c] (%)	H_2[d] (%)
Bipy (**1O**)	41	28	3	0	18	0	59	1	25	13	2	5	23	101	0	0	0	7	0	34	75
Phen (**2O**)	29	24	4	0	18	0	71	0	12	13	0	2	13	100	0	0	5	7	0	25	107
Dabipy (**3O**)	69	17	8	6	0	0	31	11	26	3	7	7	8	96	18	3	3	14	0	19	96
Daphen (**4O**)	14	30	4	0	20	0	86	0	19	14	1	6	9	101	0	0	3	11	0	24	111

[a] *Reaction conditions for all entries*: solvent: sulfolane, 500 mmol/L acetophenone, 700 psi H_2(g), 0.5 mol% catalyst load, 24 h, ISTD for GC: 100 mmol/L DMS. *Abbreviations*: AP: acetophenone, PE: 1-phenylethanol, ST: styrene, EB: ethylbenzene, BPE: bis(1-phenyl-ethyl)ether (diastereomeric mixture of (*S*,*S*/*R*,*R*) and (*R*,*S*), DPB: 1,3-diphenyl-1-butene, H_2 eq.: total hydrogenation equivalents consumed (in % relative to initial AP).

[b] By quantitative GC with multi-level calibration against authentic samples.

[c] Approximate by quantitative GC using the same response factor as for acetophenone. Value as percentage of acetophenone equivalents, i.e., %BPE: [(final BPE concentrated/2)/(initial AP concentrated)] × 100% and %DPB: [(final DPB concentrated/2)/(initial AP concentrated)] × 100%.

[d] Calculated as total hydrogenation equivalents consumed in % relative to initial AP, i.e., $\%H_2 = 100\% - \%AP + \%EB$. This value can be >100% due to the secondary hydrogenation of styrene to ethylbenzene.

Table 6
Hydrogenation of benzophenone by $[Ru(H_2O)(N \cap N)(p\text{-Me-}^iPrC_6H_4)](OTf)_2$, N ∩ N = bipy, dabipy, phen or daphen

N ∩ N[a]	T [°C]																			
	50							70							90						
	BP (%)	DOH (%)	DPM (%)	BPME (%)	MB (%)	H_2 (%)		BP (%)	DOH (%)	DPM (%)	BPME (%)	MB (%)	H_2 (%)		BP (%)	DOH (%)	DPM (%)	BPME (%)	MB (%)	H_2 (%)	
Bipy (**1O**)	62	9	0	23	71	38		16	21	23	41	60	108		1	1	96	1	98	194	
Bipy (**1O**)[b]	–	–	–	–	–	–		–	–	–	–	–	–		0	5	81	14	86	181	
Bipy (**1O**)[c]	–	–	–	–	–	–		–	–	–	–	–	–		0	80	0	20	100	0	
Phen (**2O**)	66	14	1	19	81	35		15	30	14	41	59	99		2	10	80	7	92	177	
Dabipy (**3O**)	96	1	0	3	97	4		96	1	3	0	100	7		86	1	12	2	99	27	
Dabipy (**3O**)[d]	–	–	–	–	–	–		91	0	3	5	94	11		–	–	–	–	–	–	
Daphen (**4O**)	97	1	0	2	98	3		82	6	5	6	93	22		54	7	33	7	94	80	

[a] *Reaction conditions*: solvent: sulfolane, 500 mmol/L benzophenone, 700 psi H2(g), 0.5 mol% catalyst load, 24 h, ISTD for GC: 100 mmol/L DMS. *Abbreviations*: BP: benzophenone, DOH: diphenylmethanol, DPM: diphenylmethane, BPME: bis(diphenylmethyl) ether (not analyzable by GC due to decomposition), MB: mass balance exclusive BPME, %DPOH: [(final DPOH concentrated)/(initial benzophenone concentrated)] × 100%, %DPM = [(final DPM concentrated)/(initial benzophenone concentrated)] × 100%, %BPME = BP(initial) − %BP − %DPOH − %DPM, %MB = %BP + %DPOH + %DPM, $\%H_2 = \%DPOH + 2 \times \%DPM + BPME$ (amount of H_2 consumed relative to BP can be higher than 100% due to formation of DPM), "–": not determined.

[b] Run conducted using DOH as the substrate.

[c] Baseline run conducted using DPOH as the substrate without metal catalyst.

[d] A run conducted with the addition of 4 equivalents of HOTf with respect to catalyst.

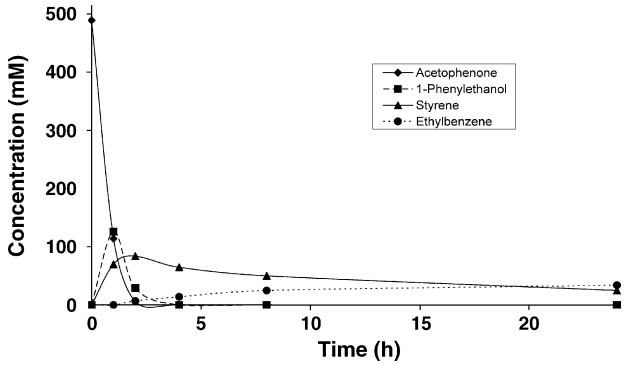

Fig. 5. Concentration/time profile of acetophenone hydrogenation by **2O[OTf]$_2$** at 90 °C.

effective *metal–ligand bifunctional* hydrogenation mechanism. For the hydrogenation of the sterically more demanding benzophenone the aminated catalysts were consistently much less active, suggesting that the presence of the amine substituents substantially hinders substrate access to the ruthenium centre. This again also implies that a concerted proton/hydride transfer mechanism as proposed in Scheme 3 does not operate. Instead a direct coordination of the substrate to the ruthenium, likely through an insertion of a carbonyl or alkene into the Ru–H bond, is required. The addition of 4 equivalents (w.r.t. ruthenium) of free HOTf to a hydrogenation of benzophenone by the dabipy catalyst **3O[OTf]$_2$** (entry 6, Table 6) marginally improves the reaction outcome, i.e., it does not induce a change in mechanism leading to a more active catalysts system.

2.4. Deoxygenation of 1,2-hexanediol

As stated earlier a successful deoxygenation of terminal diols to primary alcohols by a catalyst system is a necessary – albeit not sufficient – prerequisite for a selective transformation of glycerol to 1,3-propanediol (or other sugar polyalcohols to the corresponding α,ω-diol) by the same catalyst. 1,2-Hexanediol was selected as the model system for a comparative evaluation of the catalysts **1O[OT]$_2$–8O[OTf]$_2$**. Scheme 8 shows the overall reaction cascade occurring with terminal diols under acidic conditions as previously established with 1,2-propanediol as the model substrate [14,15]. The deoxygenation of terminal diols begins with an acid-catalyzed dehydration of the diol to the corresponding aldehyde, which constitutes the actual hydrogenation substrate. Compared to 1,2-propanediol the longer chain substrate has the advantage that its total hydrogenation product hexane (cf. Scheme 1b) has a low enough volatility to be easily be quantifiable by GC using liquid samples drawn directly from the reaction mixture without any further sample preparation.

Summarized in Table 7 are the results of the evaluation of the procatalysts **1O–4O[OTf]$_2$** against 1,2-hexanediol using 12 molar equivalents of HOTf (w.r.t. ruthenium catalysts) with all other reaction conditions equivalent to those for acetophenone and benzophenone. The initial acid-catalyzed dehydration step requires an empirically determined minimum reaction temperature of 90 °C below which no diol reactivity is observed, i.e., the acid-catalyzed dehydration appears to have a higher activation barrier than the subsequent metal-catalyzed carbonyl hydrogenation, which for acetophenone and benzophenone proceeds even at 50 °C (cf. Tables 5 and 6). At 90 and 110 °C the reactions mixtures appear as clear yellow solutions at the end point of the reactions (24 h). Higher temperatures (125 °C) result in lower yields of hydrogenated materials and increased catalyst decomposition as indicated by discolouration of the reaction mixture, appearance of a black precipitate and a peak for free *p*-cymene in the GC-trace of the solutions. The maximum yield of 46% 1-hexanol and maximum consumption of H_2(g) was observed with **2O[OTf]$_2$**. As with the ketone substrates, a pairwise comparison of the catalyst pairs *bipy* vs. *dabipy* and *phen* vs. *daphen* reveals that the presence of the amino functions has a detrimental effect on overall catalyst activity, which is somewhat less pronounced for the phen systems. In all cases good selectivity to the primary alcohol and only marginal yields of hexane were observed. This is in contrast to the [*cis*-Ru(6,6′-Cl$_2$-2,2′-bipy)$_2$(OH$_2$)$_2$][OTf]$_2$ catalyst that we previously evaluated under similar conditions. Under almost identical reaction conditions this catalyst yielded 29% 1-hexanol and 33% hexane [15].

The increase of the water concentration in the reaction mixture as the reaction progresses demands an evaluation of the

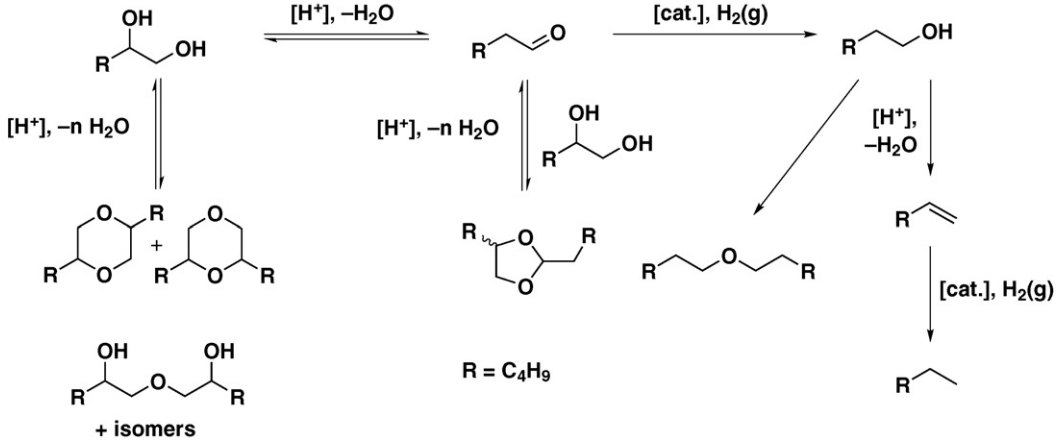

Scheme 8. Reaction cascade for the deoxygenation of 1,2-diols under acidic conditions.

Table 7
Deoxygenation of 1,2-hexanediol by $[Ru(H_2O)(N \cap N)(p\text{-Me-}^{i}PrC_6H_4)](OTf)_2$, N ∩ N = bipy, dabipy, phen or daphen

N ∩ N[a]	1,2-HD (%)[b]	1-HOL (%)[b]	2-HOL (%)[b]	HAL (%)[b]	HEX (%)[b]	DHE (%)[b]	1,3-DO (%)[b]	1,4-DO (%)[b]	DE[c] (%)[b]	MB (%)[b]	H_2[d] (%)[b]
$T = 90\,^{\circ}C$											
Bipy (**1O**)	26	32	0	1	0	0	7	0	33	67	32
Phen (**2O**)	34	28	0	0	0	1	3	5	29	71	30
Dabipy (**3O**)	10	9	1	4	0	0	10	7	59	41	10
Daphen (**4O**)	20	25	1	2	0	0	5	5	42	58	26
$T = 110\,^{\circ}C$											
Bipy (**1O**)	0	26	0	0	1	1	2	0	70	30	29
Phen (**2O**)	2	46	0	0	1	2	4	3	42	58	50
Dabipy (**3O**)	0	14	0	0	1	0	2	0	82	18	17
Daphen (**4O**)	1	35	1	0	2	2	63	0	56	44	40

[a] *Reaction conditions for all entries*: solvent: sulfolane, 500 mmol/L 1,2-hexanediol, 30 mmol L^{-1} HOTf (12.0 eq. w.r.t. catalyst), 700 psi H_2(g), 0.5 mol% catalyst load, 24 h, ISTD for GC: 100 mmol/L DMS. *Abbreviations*: 1-HD: 1,2-hexanediol, 1-HOL: 1-hexanol, 2-HOL: 2-hexanol, HAL: hexanal, HEX: hexane, DHE: *n*-dihexyl-ether, 1,3-DO: 1-pentyl-3-butyl-1,3-dioxolane,2,5(6)-di-butyl-1,4-dioxane, DE: 1,1/1,2/2,2-diol ether, MB: mass balance of all species identified by GC.
[b] As % of 1,2-hexanediol consumed.
[c] Calculated as DE = 100% − MB (these yields are inferred as the compounds cannot be analyzed by GC).
[d] Calculated as total hydrogenation equivalents consumed in % relative to initial 1,2-HD.

effect of the relative acid and water content on catalyst activity and product distribution (Scheme 8). Employing the most active catalyst identified (**2O**), The influence of the amount of water added to the reaction mixture (in weight% with respect to the total amount of sulfolane/water mixture) at the beginning of the reaction on the yield of 1-hexanol achieved is illustrated in Fig. 6. Reaction conditions are as defined previously (cf. footnote a, Table 7). As expected, increasingly larger amounts of water inhibit the reaction by pushing the initial dehydration equilibrium back to the side of the 1,2-diol starting material, i.e., the yield is increasingly limited due to the thermodynamics of this reaction. An interesting – and reproducible – feature is the slight increase in observed yield upon addition of 1 mol% water, which points to a possible catalyst activation induced by the presence of water in the reaction mixture lending support to the hydrogen activation pathway proposed by Ogo and co-workers [19] shown in the top of Scheme 5.

Shown in Fig. 7 is the effect of the amount of HOTf added (in mol equivalents relative to ruthenium catalyst) on the achievable yield of 1-hexanol in the catalytic deoxygenation of 1,2-hexanediol with **2O[OTf]$_2$**. As the graph shows a maximum yield of the primary deoxygenation product 1-hexanol is achieved with 8 equivalents, while higher amounts give no further improvement and with increasing acid concentration ultimately lead to catalyst decomposition. The optimal acid concentration thus represents a compromise between the acidity that is required for an efficient dehydration of the diol to the actual aldehyde hydrogenation substrate and the catalyst stability and selectivity under acidic conditions.

Overall catalyst activity and selectivity for the deoxygenation of the model system and ultimately glycerol or other sugar alcohols is however much more complex and a function of at least 7 parameters:

1. the catalyst concentration;
2. the substrate concentration;
3. the solvent and its relative concentration;
4. temperature;
5. hydrogen pressure;
6. initial acid concentration (i.e., equivalent of acid added);
7. initial water concentration (i.e., initial water content of the reaction mixture).

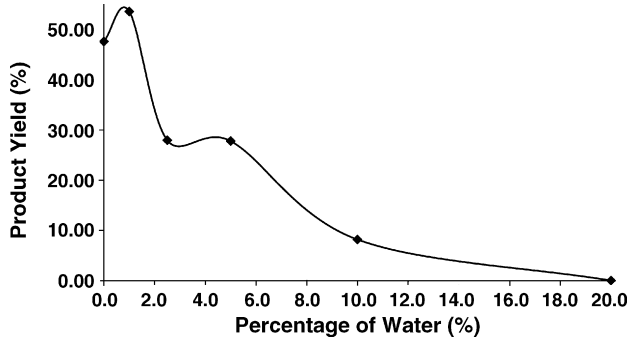

Fig. 6. Effect of the amount of water added (in weight% relative to total amount of sulfolane/water mixture) on the yield of 1-hexanol in the catalytic deoxygenation of 1,2-hexanediol with **2O[OTf]$_2$** at 4 equivalents of HOTf w.r.t. ruthenium catalyst.

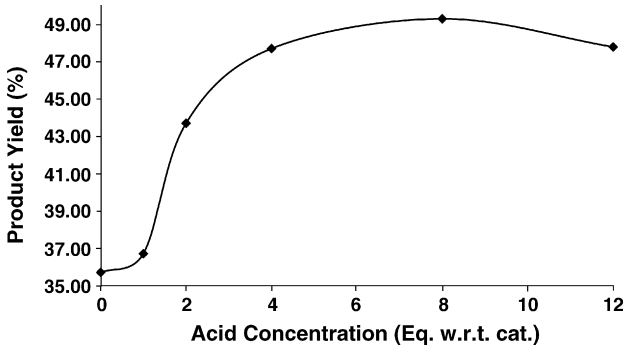

Fig. 7. Effect of the amount of HOTf added (in mol equivalents relative to ruthenium catalyst) on the achievable yield of 1-hexanol in the catalytic deoxygenation of 1,2-hexanediol with **2O[OTf]$_2$**.

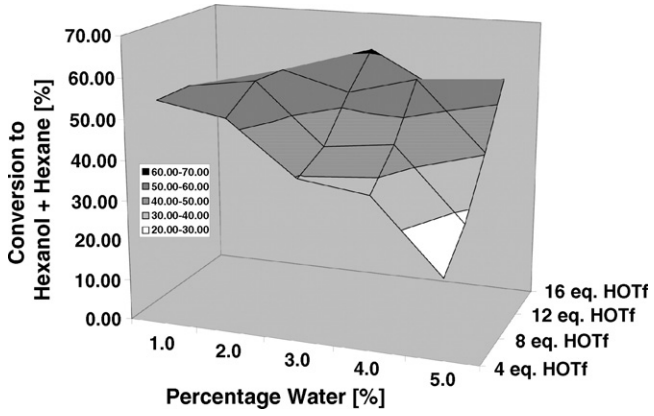

Fig. 8. Combined effects of acid and water content on the achievable yield of 1-hexanol and hexane in the catalytic deoxygenation of 1,2-hexanediol with **2O[OTf]$_2$**.

These parameters can be viewed as defining a 7-dimensional "reaction-yield space" the optimum of which can only be determined empirically. From the complex reaction cascades that evolve under the acidic conditions for both the model as well as glycerol substrates [2,14,15], it is also immediately evident that parameters 2, 3 and in particular 6 and 7 are not independent of each other, as the relative concentrations are not only determined by their initial values, but also by all chemical processes – reversible (i.e., equilibria) and irreversible (i.e., kinetically and thermodynamically competent to final products) – in the reaction mixture. While a simultaneous variation of all four (let alone all seven!) reaction parameters is technically not feasible, the use of a parallel reactor allows the systematic and simultaneous variation of two parameters effectively mapping out the "reaction-yield space" in two dimension. Using the procatalyst **1O[OTf]$_2$**, Fig. 8 shows the result of such a two-dimensional experiment for parameters 6 and 7, ranging from 0, 4, 8 to 16 equivalents of initial acid/ruthenium and 0–5% initial water content. Using a 24 well parallel reactor with 4 wells serving as controls a 4 × 5 array results showing a maximum yield of 61% for the combination 16 eq. HOTf and 3% water. This a very different result than what would have been predicted from a simple linear combination of the corresponding one-dimensional experiments shown in Figs. 6 and 7.

Listed in Table 8 are lists the optimum acid/water ratios determined for all procatalysts **1O–8O[OTf]$_2$**. No clear trend for an optimum ratio emerges from the data, but the results again show that the aminated ligands give lower yields. In one case (**4O**), where the yield approaches that of the non-aminated parent system, catalyst decomposition is observed as indicated by discolouration of the solution and formation of a black precipitate. The *p*-cymene complexes **1O** and **2O** achieve higher conversions than the corresponding C_6Me_6 complexes **5O** and **6O**—this is the opposite trend of what was observed by Süss-Fink and co-workers [17,18] in the transfer hydrogenation of acetophenone by the same complexes in biphasic media at pH 3.8. Their study notes a pronounced increase in catalytic activity with increasing alkyl substitution on the η^6-arene ring from C_6H_6 to *p*-cymene to C_6Me_6. The origin of this discrepancy must lie in the very different reaction conditions employed: the transfer hydrogenation was carried out at 50 °C using formic acid as the reductant, while the hydrogen gas hydrogenation was carried out at 110 °C. Either or both of these differences alone could result in a different mechanism with a different rate-determining step.

2.5. Control experiments for homogeneity

Previous work by Finke and co-workers had shown that ruthenium(II) η^6-arene complexes, in particular those lacking further supporting ligands, can serve as a source of highly catalytically active ruthenium nano-particles formed by auto-catalytic reduction to ruthenium(0) in situ [41]. For the N ∩ N ligand stabilized catalytically active ruthenium centres described here we exclude this possibility on the basis of the following observations: in almost all reactions very small amounts (<1 mg) of black residue form, but this residue is not catalytically active, i.e., decanting from this residue and recharging the reactor without cleaning between catalytic runs does not give catalytic activity

Table 8
Empirically determined optimum initial acid/water content of the reaction mixture for the deoxygenation of 1,2-hexanediol by complexes **1O–8O**

#[a]	N ∩ N	η^6-arene	Eq. HOTf	%H_2O	HOTf/H_2O	Yield [%][b]
1O	Bipy	*p*-Cymene	12	2	6	63
2O	Phen	*p*-Cymene	16	3	5.3	61
3O	Dabipy	*p*-Cymene	8	1	8	24[c]
4O	Daphen	*p*-Cymene	8	2	4	59[c]
5O	Bipy	C_6Me_6	12	4	4	48[d]
5O			16	5	3.2	48
6O	Phen	C_6Me_6	16	4	4	51[d]
7O	Dabipy	C_6Me_6	8	3	2.6	25
8O	Daphen	C_6Me_6	4	1	4	29
8O			12	4	3	29
8O			16	5	3.2	29

[a] *Reaction conditions for all entries*: solvent: sulfolane, 500 mmol/L 1,2-hexanediol, 110 °C, 1100 psi H_2(g), 0.5 mol% catalyst load, 24 h, ISTD for GC: 100 mmol/L DMS.
[b] Combined yield of 1-hexanol and hexane (the latter is ≤2% in all cases).
[c] Catalyst was decomposed at the end of the reaction.
[d] No hexane formation observed.

Table 9
Reaction conditions explored in the attempted deoxygenation of glycerol by **2O[OTf]$_2$**

Conditions[a]				Comments
Reaction #	Acid (w.r.t. catalyst)	Water (%)	Temperature (°C)	
1	4.0 eq. HOTf	1	110	No reaction
2	8.0 eq. HOTf	1	110	No reaction
3	4.0 eq. HOTf	–	110	No reaction
4	12.0 eq. HOTf	–	110	No reaction
5	4.0 eq. HOTf	–	125	Catalyst decomposition
6	8.0 eq. HOTf	–	175	Catalyst decomposition
7	4.0 eq. H_2WO_4	–	110	No reaction
8	12 eq. H_2WO_4	–	175	Catalyst decomposition

[a] *Reaction conditions*: solvent: sulfolane, 700 psi H_2(g), 500 mmol L^{-1} glycerol, 2.5 mmol L^{-1} catalyst (0.5 mol%), 100 mmol L^{-1} DMS (internal GC standard), t = 24 h.

beyond the base activity of the reactor vessel itself (typically <1% conversion). The same black precipitate is also observed in blank reactions, i.e., reactions in which no catalyst added and is therefore likely organic in nature. The blank reactions showed no catalytic activity. In catalytic reactions where more pronounced catalyst decomposition was observed (notably with **3O** and **4O**) the observed yields were always much lower than in those reactions where no catalysts decomposition occurred. Finally, using the analogous P ∩ P complexes as hydrogenation catalysts for styrene under comparable conditions, Dyson and co-workers established that no decomposition to active heterogeneous species occurs [35].

2.6. Attempted deoxygenation of glycerol

Upon examination of the reaction parameters associated with the model system 1,2-hexanediol, reactions with glycerol as the deoxygenation substrate were carried out. The procatalyst **2O[OTf]$_2$** was employed using a range of acid and water concentrations and reaction temperatures. However, GC analysis of the reaction mixture showed no detectable amount of 1,3-propanediol or any other deoxygenation products. Following the reaction conditions employed with the benchmark rhodium catalyst patented by Celanese [3], tungstic acid (H_2WO_4) was also tested as the acid-catalyst, again with no success. The reaction conditions employed in the attempts to reduce glycerol are summarized in Table 9.

The initial attempt in the deoxygenation of glycerol employed the optimum conditions determined for the reduction of 1,2-hexanediol with procatalyst **2O[OTF]$_2$** in the water series, i.e., 4 eq. HOTf with 1% water/sulfolane solvent (first entry, Table 9). A sample taken from the reaction at t = 0 h was analyzed by GC and showed the presence of glycerol and two unknown species, the identities of which could not be established by GC–MS, but were hypothesized to be acid-catalyzed glycerol condensation products, as reaction samples taken later showed a decrease in concentration of these two species and an increase in the glycerol concentration with time. After 24 h the only species present in the reaction mixture was glycerol and the mass balance of the reaction accounted for all of the glycerol initially present. Reactions 2–4, which employed either a higher acid concentration or pure sulfolane as the reaction solvent, yielded the same results as those of Reaction 1. Since no reactivity was observed at 110 °C, higher reaction temperatures, 125 and 175 °C, were used in reactions 5 and 6 as it was postulated that the activation energy barrier for the initial dehydration of glycerol was not being overcome at 110 °C. Analogous to the observations with the diol model substrate, at 125 or 175 °C, the reaction mixture went from an orange-yellow to a green and ultimately colourless solution with the presence of black precipitate, signifying decomposition of the catalyst. Again, glycerol was the only species present after 24 h. However, the final mass balance could only account for 38% of the initial substrate concentration for Reaction (5) and no detectable amount of glycerol was present in Reaction*** 6 after 24 h. Therefore, these higher reaction temperatures promoted the condensation of glycerol to species that could not be detected by GC, most likely the formation of acid-catalyzed dimeric or oligomeric species similar to those formed by the condensation of diols (cf. Scheme 8 and Ref. [2]). Only very small amounts of acrolein were observed during the course of these analyses. Reactions 7 and 8 which used H_2WO_4 as the acid-catalyst gave similar results.

3. Discussion

To our knowledge no thermodynamic data on the acid-catalyzed condensation behaviour of glycerol in aqueous and/or sulfolane solution exist. A recent theoretical study on the acid-catalyzed dehydration of glycerol in the gas phase [42] reports activation barriers of ∼25 kcal/mol for a pinacol rearrangement type hydride shift mechanism to protonated 3-HPA and ∼37 kcal/mol for loss of water to form the secondary carbocation $HOCH_2CH^+CH_2OH$. While these barriers can be anticipated to be substantially lower in a highly polar medium capable of stabilizing charged intermediates, they still appear to be high enough that under the reaction conditions accessible by the catalysts (i.e., $T \leq 110$ °C) the prerequisite initial dehydration of glycerol does not proceed, in particular if one considers the carbocation pathway. The origin of the difference in behaviour between the terminal diols and glycerol is unclear. An additional catalyst design criterion emerges from these realizations. The catalyst must be of high thermal stability, i.e., be active at reaction temperatures of at least 175 °C. This constitutes an interesting challenge for a homogeneous system that may how-

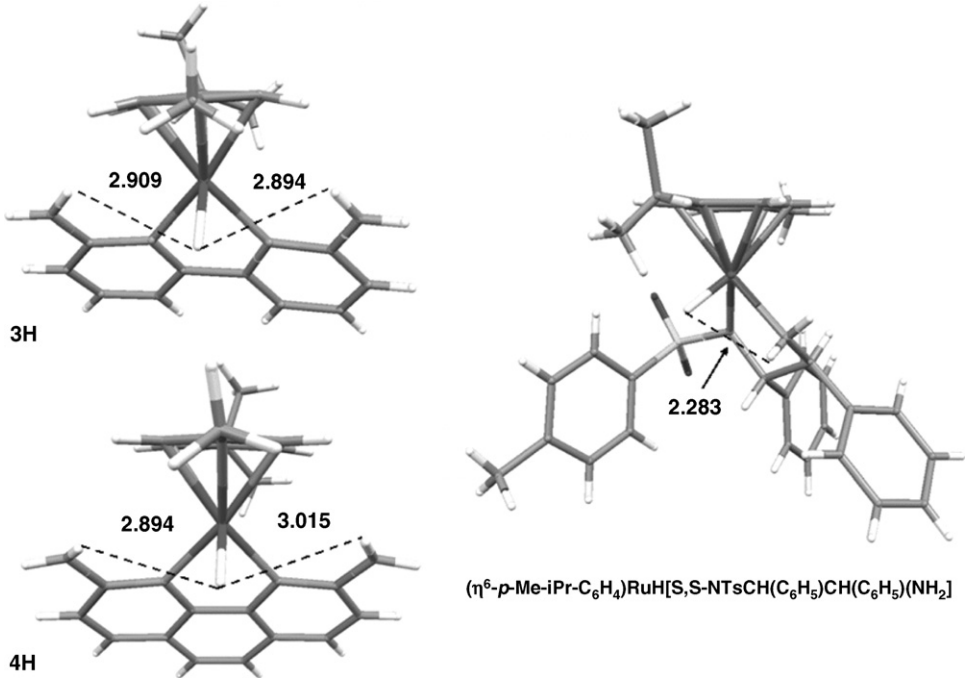

Fig. 9. Comparison of proton–hydride distances (in Å) in **3H** and **4H** with that in the Noyori catalyst (η^6-*p*-Me-^{i}Pr-C_6H_4)Ru(H)[*S*,*S*-NTsCH(C_6H_5)CH(C_6H_5)NH_2].

ever be surmountable by designing catalysts employing tri- or tetradentate ligand frameworks, which should result in thermally more stable catalysts. In this context it is noteworthy that both homogeneous glycerol deoxygenation catalyst systems reported in the patent literature [3,4] operate under an atmosphere of synthesis gas rather than pure hydrogen. The resulting presence of carbonyl ligands likely serves to protect the metal centre from reduction under the forcing reaction conditions (T = 175–200 °C).

The failure of the amino substituted procatalysts **3O[OTf]$_2$**, **4O[OTf]$_2$**, **7O[OTf]$_2$** and **8O[OTf]$_2$** to show higher activity induced by a metal–ligand bifunctional mechanism can be traced to at least two factors: (1) The low pK_a of a protonated amino function in coordinated dabipy or daphen. (2) A mismatch between the proton–hydride distance in the hydrogen loaded catalyst. For both factors a comparison to the Noyori catalyst is instructive, as it is the only system for which structural data and a consensus on a metal–ligand bifunctional mechanism exists. Experimental results suggest a p$K_a < -2$ for the protonated amino functions in the monocationic catalysts, while due to the condensation chemistry the strongest acid possible acid in the reaction mixtures is H_3O^+ with a pK_a of −1.74 (values extrapolated to pure aqueous medium) [38]. The low p*K*a of the protonated ligand thus closely matches the solvent level of the aqueous medium (cf. Fig. 4) and is relatively close to the pK_a of the ketone and ether hydrogenation/hydrogenolysis targets, which in their protonated form have estimated pK_a of −7 to −3.5 on an aqueous scale. However, as the example of the Noyori system shows and which in fact operates under basic conditions [29,43,44], an actual protonation of the substrate may not be necessary in order to effect a metal–ligand bifunctional proton–hydride transfer to an unsaturated substrate. A similar observation has been made for the Shvo system [45], which also has been shown to act as a *metal–ligand* bifunctional catalyst, effecting hydrogenation by a proton/hydride transfer mechanism and for which the pK_a of the proton donor tetraphenyl-hydroxyl-cyclopentadienyl has been determined to be 17.5 in acetonitrile, which may roughly correlate to a pK_a = 4 in aqueous media [24]. In both cases the desired proton/hydride transfer mechanism is thus better formulated through a concerted transition state [29,46], in which the relative pK_a value of the proton shuttle on the catalyst and the protonated substrate is only one of several factors. In this scenario the more critical parameter is not the pK_a of the proton donor, but more likely the distance between the proton and hydride donor in the coordination sphere of the catalytic metal centre. Fig. 9 compares the structures of the hydride complexes **3H** and **4H** with that of the structurally similar Noyori system (η^6-*p*-Me-^{i}Pr-C_6H_4)Ru(H)[*S*,*S*-NTsCH(C_6H_5)CH(C_6H_5)NH_2] [44]. The Ru–H···H–N distance of 2.29 Å in the Noyori system is shorter than the van der Waals distance of 2.4 Å, suggesting the existence of a weak hydrogen bond interaction. The corresponding distances in the metal–ligand bifunctional systems reported by Morris, e.g. *trans*-Ru(H)$_2$(R-binap)(tmen) (tmen = tetramethyl ethylene diamine) are ∼2.4 Å, i.e., "at the outer limit of protonic–hydridic or dihydrogen bonding" [27,28]. Even though the steric repulsion between the amino substituents and the η^6-arene ligand serve to bring the NH_2-protons closer to the hydride ligand (cf. Fig. 2 and angle α in Table 2), the corresponding distances in **3H** and **4H** are ∼2.9 Å, i.e., substantially longer by ∼0.5–0.6 Å. Considering that the average C=O distance in the carbonyl hydrogenation targets is ∼1.43 Å this further suggest that the proton–hydride distances in the amino-substituted bipy and phen complexes 3H and 4H are too long to allow a

metal–ligand bifunctional proton/hydride transfer mechanism. A further difference between the Noyori and Morris catalysts and the systems described here is the extent of electronic coupling between the hydride and proton source, e.g., in (η^6-*p*-Me-^{i}Pr-C_6H_4)Ru(H)[*S*,*S*-NTsCH(C_6H_5)CH(C_6H_5)NH_2] the proton donating amine function is coordinated, which substantially lowers its pK_a, and cycles between NH_2 in the hydrogen loaded 18 electron complex and NH in the hydrogen deficient 16 electron complex [29]. In contrast there is no or only a very weak and remote electronic connection between the proton and hydride source in the hydride complexes **3H**, **4H**, **7H** and **8H** and the pK_a of the unprotonated amino function is too high for them to serve as proton sources. As the example of the Shvo system shows, coordination of the proton source to the active metal centre is however not an absolutely necessary condition for metal–ligand bifunctionality.

4. Conclusions

The complexes [(η^6-arene)Ru(H_2O)(N∩N)]$(OTf)_2$, η^6-arene = *p*-Me-^{i}Pr-C_6H_4, C_6Me_6, N∩N = bipy, phen, 6,6′-diamino-bipy, 2,9-diamino-phen) form active catalysts for the hydrogenation of ketones in sulfolane. Under acidic conditions that promote dehydration they selectively deoxygenate terminal diols to the corresponding primary alcohols by hydrogenating the intermediate aldehyde. The product distributions and catalyst activities are a complex function of the initial water and acid (HOTf) content of the reaction mixtures. The catalysts are inactive for the deoxygenation of glycerol to 1,3-propanediol or other products, as they do not sustain the temperatures required for an initial acid-catalyzed dehydration of glycerol to 3-hydroxy-propionaldehyde (estimated to be >150 °C). The amino substituents introduced into the *ortho*-positions of the chelating ligands do not result in higher catalyst activity, i.e., they fail to act as proton donors in a hypothesized metal–ligand bifunctional proton/hydride transfer mechanism to the carbonyl substrates. This is likely caused by a mismatch between the proton/hydride distance in the catalysts and the C=O distance in the carbonyl hydrogenation targets.

5. Supplementary material

Full experimental details: NMR data and spectrum images for all complexes synthesized. Crystallographic data (excluding structure factors) for the structures reported in this paper have been deposited with the Cambridge Crystallographic Data Centre as supplementary publication no. CCDC-652579 (**3Cl[BF_4]**), CCDC-652580 (**3H[OTf]**), CCDC-652581 (**3O[$OTf]_2$**), CCDC-652582 (**3O[SO_4]**), CCDC-652583 (**4Cl[Cl]**), CCDC-652584 (**4H[OTf]**), CCDC-652585 (**4O[$OTf]_2$**, CCDC-652586 (**7Cl[Cl]**), CCDC-652587 (**7H-BH_2-OTf**), CCDC-652588 (**8Cl[OTf]**) (from MeOH), CCDC-652589 (**8Cl[OTf]**) (from acetone), CCDC-652590 (**8O(MeOH)[$OTf]_2$**), CCDC-652591 (**1O[$OTf]_2$**). Copies of the data can be obtained free of charge on application to CCDC, 12 Union Road, Cambridge CB2 1EZ, UK [fax: +44 1223 336-033; e-mail: deposit@ccdc.cam.ac.uk].

Acknowledgements

This work was supported by the Natural Science and Engineering Research Council of Canada (NSERC), the Canadian Foundation for Innovation (CFI), Natural Resources Canada, (NRCAN), the Ontario Ministry of Agriculture, Food and Rural Affairs (OMAFRA), the BioCap Canada Foundation and DuPont.

Appendix A. Supplementary data

Supplementary data associated with this article can be found, in the online version, at doi:10.1016/j.molcata.2007.08.008.

References

[1] M. McCoy, CEN News 83 (2005) 19–20.
[2] M. Schlaf, J. Chem. Soc., Dalton Trans. (2006) 4645–4653.
[3] T. Che, Production of Propanediols, Celanese Corporation, US 4,642,394 (1987).
[4] E. Drent, W.W. Jager, Hydrogenolysis of Glycerol, Shell Oil, US 6,080,898, W 9,905,085 (2000).
[5] Y. Kusunoki, T. Miyazawa, K. Kunimori, K. Tomishige, Catal. Commun. 6 (2005) 645–649.
[6] T. Miyazawa, Y. Kusunoki, K. Kunimori, K. Tomishige, J. Catal. 240 (2006) 213–221.
[7] M.A. Dasari, P.P. Kiatsimkul, W.R. Sutterlin, G.J. Suppes, Appl. Catal. A 281 (2005) 225–231.
[8] A. Perosa, P. Tundo, Ind. Eng. Chem. Res. 44 (2005) 8535–8537.
[9] T. Miyazawa, S. Koso, K. Kunimori, K. Tomishige, Appl. Catal. A 318 (2007) 244–251.
[10] M. McCoy, Chem. Eng. News 85 (2007) 7.
[11] C.W. Chin, M.A. Dasari, G.J. Suppes, W.R. Sutterlin, AlChE J. 52 (2006) 3543–3548.
[12] S. Vollenweider, G. Grassi, I. Konig, Z. Puhan, J. Agric. Food. Chem. 51 (2003) 3287–3293.
[13] S. Vollenweider, C. Lacroix, Appl. Microbiol. Biotechnol. 64 (2004) 16–27.
[14] M. Schlaf, P. Gosh, P.J. Fagan, E. Hauptman, R.M. Bullock, Angew. Chem., Int. Ed. 40 (2001) 3887–3890.
[15] Z. Xie, M. Schlaf, J. Mol. Catal. A: Chem. 229 (2005) 151–158.
[16] S. Ogo, T. Abura, Y. Watanabe, Organometallics 21 (2002) 2964–2969.
[17] J. Canivet, L. Karmazin-Brelot, G. Süss-Fink, J. Organomet. Chem. 690 (2005) 3202–3211.
[18] P. Stepnicka, J. Ludvik, J. Canivet, G. Süss-Fink, Inorg. Chim. Acta 359 (2006) 2369–2374.
[19] H. Hayashi, S. Ogo, S. Fukuzumi, Chem. Commun. (2004) 2714–2715.
[20] H. Hayashi, S. Ogo, T. Abura, S. Fukuzumi, J. Am. Chem. Soc. 125 (2003) 14266–14267.
[21] S. Ogo, R. Kabe, H. Hayashi, R. Harada, S. Fukuzumi, J. Chem. Soc., Dalton Trans. (2006) 4657–4663.
[22] Y. Blum, D. Czarkie, Y. Rahamin, Y. Shvo, Organometallics 4 (1985) 1459–1461.
[23] Y. Shvo, D. Czarkie, Y. Rahamin, J. Am. Chem. Soc. 108 (1986) 7400–7402.
[24] C.P. Casey, S.W. Singer, D.R. Powell, R.K. Hayashi, M. Kavana, J. Am. Chem. Soc. 123 (2001) 1090–1100.
[25] R. Abbel, K. Abdur-Rashid, M. Faatz, A. Hadzovic, A.J. Lough, R.H. Morris, J. Am. Chem. Soc. 127 (2005) 1870–1882.
[26] K. Abdur-Raschid, R. Abbel, A. Hadzovic, A.J. Lough, R.H. Morris, Inorg. Chem. 44 (2005) 2483–2492.
[27] K. Abdur-Rashid, S.E. Clapham, A. Hadzovic, J.N. Harvey, A.J. Lough, R.H. Morris, J. Am. Chem. Soc. 124 (2002) 15104–15118.
[28] K. Abdur-Rashid, M. Fraatz, A.J. Lough, R.H. Morris, J. Am. Chem. Soc. 123 (2001) 7473–7474.

[29] R. Noyori, M. Yamakawa, S. Hashiguchi, J. Org. Chem. 66 (2001) 7931–7944.
[30] M. Yamakawa, H. Ito, R. Noyori, J. Am. Chem. Soc. 122 (2000) 1466–1478.
[31] L. Dadci, H. Elias, U. Frey, A. Hoernig, U. Koelle, A.E. Merbach, H. Paulus, J.S. Schneider, Inorg. Chem. 34 (1995) 306–315.
[32] R. Zelonka, M.C. Baird, Can. J. Chem. 50 (1972) 3063–3072.
[33] M.A. Bennett, T.-N. Huang, T.W. Matheson, A.K. Smith, in: J.P. Fackler (Ed.), Inorganic Synthesis, John Wiley & Sons, New York, 1982, pp. 74–77.
[34] M. Stebler-Röthlisberger, A. Ludi, Polyhedron 5 (1986) 1217–1221.
[35] C. Daguenet, R. Scopelliti, P.J. Dyson, Organometallics 23 (2004) 4849–4857.
[36] D.G. Hamilton, R.H. Crabtree, J. Am. Chem. Soc. 110 (1988) 4126–4133.
[37] G. Kubas, Metal Dihydrogen and σ-Bond Complexes. Structure, Theory and Reactivity, Kluwer Academic/Plenum Publishers, New York, 2001.
[38] M.L. Campbell, B.A. Waite, J. Chem. Ed. 67 (1990) 386–388.
[39] S. Ogo, K. Uehara, T. Abura, Y. Watanabe, S. Fukuzumi, Organometallics 23 (2004) 3047–3052.
[40] C. Waterlot, D. Couturier, M. De Backer, B. Rigo, Can. J. Chem. 78 (2000) 1242–1246 (and references therein).
[41] J.A. Widegren, M.A. Bennett, R.G. Finke, J. Am. Chem. Soc. 125 (2003) 10301–10310.
[42] M.R. Nimlos, S.J. Blanksby, X. Qian, M.E. Himmel, D.K. Johnson, J. Phys. Chem. A 110 (2006) 6145–6156.
[43] R. Noyori, S. Hashigushi, Acc. Chem. Res. 30 (1997) 97–102.
[44] K.-J. Haack, S. Hashiguchi, A. Fujii, T. Ikariya, R. Noyori, Angew. Chem. Int. Ed. Engl. 36 (1997) 285–288.
[45] N. Menashe, Y. Shvo, Organometallics 10 (1991) 3885–3891.
[46] C.P. Casey, J.B. Johnson, J. Org. Chem. 68 (2003) 1998–2001.